New particle formation leads to enhanced cloud condensation nuclei concentrations at Antarctic Peninsula

Jiyeon Park[1], Hyojin Kang[1,2], Yeontae Gim[1], Eunho Jang[1,2], Ki-Tae Park[1], Sangjong Park[1], Chang Hoon Jung[3], Darius Ceburnis[4], Colin O'Dowd[4], and Young Jun Yoon[1, *]

[1]Korea Polar Research Institute, 26 Songdomirae-ro, Yeonsu-gu, Incheon 21990, South Korea
[2]University of Science and Technology (UST), 217 Gajeong-ro, Yuseong-gu, Daejeon, Republic of Korea
[3]Department of Health Management, Kyungin Women's University, Incheon 21041, Republic of Korea
[4]School of Natural Sciences and Centre for Climate and Air Pollution Studies, Ryan Institute, University of Galway, Ireland
*Correspondence to: Y.J. Yoon (yjyoon@kopri.re.kr)

Abstract

Few studies have investigated the impact of new particle formation (NPF) on cloud condensation nuclei (CCN) in remote Antarctica, and none has elucidated the relationship between NPF and CCN production. To address that knowledge gap, we continuously measured the number size distribution of 2.5–300 nm particles and CCN number concentrations at King Sejong Station in the Antarctic Peninsula from January 1 to December 31, 2018. Ninety-seven new particle formation (NPF) events were detected throughout the year. The estimated median spatial scale of NPF around Antarctic peninsula was found to be approximately 155 km, indicating the large-scale of NPF events. Air back-trajectory analysis revealed that 80 cases of NPF events were associated with air masses originating over the ocean, followed by sea ice (12 cases), multiple (3 cases), and land (2 cases) regions. We present and discuss three major NPF categories: (1) marine NPF (2) sea ice NPF, and (3) multiple NPF. Our results showed that the photo-oxidation of oceanic biogenic precursors such as dimethyl sulfide (DMS) could be a key component in marine NPF events, whereas halogen compounds released from ice-covered areas could contribute to sea-ice NPF events. Terrestrial sources (wild life colonies, vegetation, and meltwater ponds) from Antarctica could affect aerosol production in multiple air masses. Out of 97 observed NPF events, 83 cases were characterized by the simultaneous increase in the CCN concentration by 2–270% (median 44%) in the

30   following 1 to 36 hours (median 8 hours) after NPF events. Overall, Antarctic NPF events were found to

31   be a significant source of particles with different physical characteristics and related to biogenic sources

32   in and around the Antarctic Peninsula, which subsequently grew to cloud nuclei.

34   **1. Introduction**

35   Antarctic peninsula is warming more rapidly than Earth's global mean rate (Chen et al., 2009;

36   Vaughan et al., 2003), leading to shrinking sea ice coverage and consequent sea-level rise (Pritchard et

37   al., 2009). In the Antarctic region, ambient aerosols play a crucial role in governing radiative transfer,

38   directly by the scattering and absorption of solar radiation and indirectly by acting as cloud condensation

39   nuclei (CCN) (IPCC, 2013). The magnitude of the radiative forcing caused by the interactions between

40   aerosols and CCN remains highly uncertain due to a poor understanding of pristine natural aerosols

41   (Carslaw et al., 2013). To reduce this uncertainty, the physicochemical properties of aerosol particles (e.g.,

42   number concentrations, size distributions, chemical compositions, and hygroscopicity) have been studied

43   at several Antarctic locations including King Sejong Station (Kim et al., 2019), Aboa (Asmi et al., 2010;

44   Virkkula et al., 2006), Dome C (Järvinen et al., 2013), Halley (Lachlan-Cope et al., 2020; O'Dowd et al.,

45   1997), Kohen (Weller et al., 2018), McMurdo (Giordano et al., 2018; Liu et al., 2018), Neumayer (Teinilä

46   et al., 2014; Weller et al., 2015), Princess Elisabeth (Herenz et al., 2019) and Syowa (Hara et al., 2011;

47   Ito, 1993), as well as from shipborne observations (Fossum et al., 2018; Humphries et al., 2015;

48   Humphries et al., 2016). Overall, aerosol particle number concentrations follow a clear annual trend,

49   being much higher in austral summer than in other seasons (Järvinen et al., 2013; Kerminen et al., 2018;

50   Weller et al., 2011). For instance, Kim et al. (2017) found that summertime concentrations in the Antarctic

51   Peninsula were ~20 times higher than in winter. This pattern can be largely explained by new particle

52   formation (NPF) events.

53   Precursor gases for NPF in this region can originate from the ocean, sea ice, meltwater ponds, and

54   terrestrial animal colonies. Oceanic emissions of dimethyl sulfide (DMS) represent the largest natural

55   sulfur source in the Antarctic atmosphere (Simó, 2001), and its photooxidation is a key process

56 contributing to NPF (Giordano et al., 2017; Jang et al., 2019 and 2022). In situ (Saiz-Lopez et al., 2007)

57 and satellite (Schönhardt et al., 2008) measurements have also shown Antarctica to be an iodine emission

58 hotspot, particularly from the sea ice in the Weddell Sea during spring (Atkinson et al., 2012). Dall´Osto

59 et al. (2017) reported that microbiota in sea ice were associated with atmospheric organic nitrogen

60 formation in the Southern Ocean near Antarctica. According to Kyrö et al. (2013), the precursor vapors

61 responsible for NPF and subsequent growth could originate from the cyanobacteria, which are abundant

62 in Antarctic meltwater ponds. In addition, continental Antarctica is a habitat for various types of seabirds

63 and penguins, with guano species acting as a crucial source of ammonia and organic compounds and may

64 contribute to NPF in coastal Antarctic areas (Schmale et al., 2013; Weber et al., 1998; Zhu et al., 2011).

65   In recent years, long-term records of aerosol size distribution have become an important aspect of

66 investigations into the sources and dynamical processes of NPF. The majority of Antarctic field studies

67 have focused on the annual and spatial patterns of the number size distribution of particles > 10 nm (Belosi

68 et al., 2012; Järvinen et al., 2013; Kim et al., 2019; Kyrö et al., 2013; Lachlan-Cope et al., 2020). Although

69 NPF events are typically characterized by a rapid increase in the number concentration of cluster from 1–

70 3 nm (Kulmala et al., 2004), datasets for these types of aerosol size distribution remain rare. To date,

71 number size distribution of particles > 3 nm has been reported by Asmi et al. (2010) at Aboa during from

72 December 29, 2006 to January 29. 2007; by Pant at al. (2011) at Maitri from January 1 to February 28,

73 2015; by Weller et al. (2015) at Neumayer from January 20 to March 26, 2012; by Jokinen et al. (2018)

74 at Aboa from November 2014 to February 2015; and by Weller et al. (2018) at Kohnen during January

75 2015 and 2016. However, all of these measurements were made during the Antarctic summer due to

76 restricted access and, therefore, limited information on seasonal cycles.

77   Newly formed particles can grow into larger sizes that act as CCN, becoming relevant for cloud

78 formation (O'Dowd, 2002; Williamson et al., 2019). In a highly pristine atmosphere such as Antarctica,

79 where CCN concentration is extremely low (Kim et al., 2017), NPF may be a significant phenomenon

80 controlling the CCN budget (Kyrö et al., 2013). For instance, Herenz et al. (2019) showed that an elevated

81 $CN_{2.5}$ (total number concentration of particles > 2.5 nm) during NPF events was accompanied by an

82   increase in CCN concentrations at Princess Elisabeth during austral summer (December to February,

83   2013–2016). In addition, seasonal variability in $CN_{2.5–10}$ (number concentration of particles within the 2.5

84   nm and 10 nm range and attributed to NPF) and CCN concentrations at King Sejong Station from March

85   2009 to December 2016 were investigated by Kim et al. (2019), who concluded that CCN concentrations

86   during NPF events increased by ~11% compared to the background concentration. However, to date, only

87   one study (Kim et al., 2019) has reported the contribution of NPF to CCN in the Antarctic Peninsula, and

88   that study did not consider aerosol number size distribution.

89   In this study, we continuously recorded the number size distribution of 2.5–300 nm particles and

90   CCN number concentrations at King Sejong Station in the Antarctic Peninsula from January 1, 2018, to

91   December 31, 2018. Our primary goals were to (1) characterize the seasonal variation and occurrence of

92   NPF events from the perspective of aerosol physical properties (total number concentration, number size

93   distribution, formation and growth rates, and condensation sink); (2) improve our understanding of the

94   major sources (including open ocean, sea ice, and land) and processes influencing NPF and particle

95   growth; and (3) estimate the contribution of atmospheric NPF to CCN activity in this pristine environment.

96   To our knowledge, this is the first study to present direct evidence of CCN production associated with

97   NPF and growth events in the Antarctic Peninsula, using simultaneous measurements of particle number

98   size distributions (down to 3 nm) and CCN properties for a full year.

99

100   **2. Experimental methods**

101   **2.1. Sampling site and instrumentation**

102   Continuous measurements of the physical properties of aerosol particles were conducted from

103   January 2018 to December 2018 at King Sejong Station in the Antarctic Peninsula (62.22° S, 58.78° W).

104   Full details of the sampling site and measurement setup are given in Kim et al. (2017). In brief, a

105   cylindrical stainless inlet (0.1 m diameter and 5.2 m length; total flow rate of the sampled air was 150 L

106   min^{-1}) was placed on the observatory roof following Global Atmosphere Watch aerosol measurement

107   guidelines and recommendations. Two condensation particle counters (TSI model 3776 CPC and TSI

108 model 3772 CPC) were used to measure the total number concentration of particles every 1 second, with

109 aerosol sample flow rates of 1.5 and 1.0 L min^{-1}, respectively. A nano-scanning mobility particle sizer

110 (nano-SMPS) consisting of a nano-differential mobility analyzer (nano-DMA) (TSI model 3085, USA)

111 and an ultrafine condensation particle counter (TSI model 3776, USA) was used to measure the number

112 size distribution of particles from 2.5–64 nm every 3 minutes. The aerosol flow rate was 1.5 L min^{-1} and

113 the sheath flow rate was 15 L min^{-1} inside the nano-DMA.

114   The particle number size distribution (from 10–300 nm every 3 min) was measured with a standard-

115 SMPS consisting of a long DMA (TSI model 3081, USA) and a CPC (TSI model 3772, USA). The aerosol

116 flow rate was 1.0 L min^{-1}, and the sheath flow rate was 10 L min^{-1} inside the long DMA. To obtain the

117 number size distribution of particles from 2.5–300 nm, the nano-SMPS and standard-SMPS were merged.

118 For particle diameters 2.5–20 nm, nano-SMPS data were chosen because this was optimized to operate

119 with a smaller particle diameter. In the nano-DMA, the aerosol residence time can be reduced by

120 shortening the inlet transport passage (5.0 cm) and increasing the inlet flow (up to 16.5 L min^{-1}) (< 10 nm)

121 (Chen et al., 1998). Hence, the number size distribution data from both nano-SMPS and standard-SMPS

122 were merged at a diameter of 20 nm. Furthermore, three-point median filter and five point moving average

123 were performed on merging the number size distribution data to remove nano-SMPS noise, as suggested

124 by Kulmala et al. (2012).

125   The black carbon (BC) concentration was measured using an aethalometer (AE22, Magee Scientific

126 Co., USA) every 5 min to examine long-range polluted aerosol transport from other continents and to

127 assess the influence of local pollution from the station. The flow rate through a sharp-cut 2.5 μm cyclone

128 (BGI, Inc., USA) was set to 5 L min^{-1}. The CCN counter (CCNC: CCN-100, Droplet Measurement

129 Technologies, USA) measured CCN number concentrations at five different supersaturations (0.2%, 0.4%,

130 0.6%, 0.8%, and 1.0%) every 30 minute. The total flow rate in the CCN counter was 0.5 L min^{-1}. The

131 sample and sheath flow rates of the CCN counter were 0.05 and 0.45 L min^{-1}, respectively. In addition,

132 basic meteorological parameters (temperature, pressure, relative humidity (RH), wind speed, wind

133 direction, and solar radiation intensity) were measured using an automatic weather station (Vaisala

134   HMP45).

135

136   **2.2. Data evaluation**

137   As the observatory is located ~400 m southwest of the main station buildings, measurement data

138   were impacted by local emissions from station activities (e.g., power generators and incineration). To

139   obtain an unperturbed aerosol population of pristine Antarctic environment, contaminated measurements

140   were removed manually based on wind direction, wind speed, BC concentration, and total particle number

141   concentration. The following data elimination procedure was applied: (1) the measurements taken within

142   wind sector of 355° and 55° were discarded as directly impacted by local pollution sources; (2) relative

143   wind speed below 2.0 m s^{-1}, as stagnant conditions would have facilitated contaminated particle

144   propagation to the measurement location; (3) equivalent BC mass concentrations exceeding 50 ng m^{-3},

145   because elevated BC concentration unambiguously pointed at polluted particles; and (4) a sharp increase

146   in the total number concentration over the entire particle diameter range in a short time scale of less than

147   an hour, as such abrupt peaks and spikes are related to potential contamination or instrumental

148   malfunctions. For instance, CPC and SMPS data were removed for time periods when particle number

149   concentrations suddenly increased to more than twice the background values.

150   Based on a four-year (2016-2019) BC dataset, six types of Antarctic Peninsula air-pollution levels

151   were identified (Grigas et al., 2017): (1) pristine air with BC concentrations < 15 ng m^{-3}, (2) clean air with

152   BC levels 15–50 ng m^{-3}, (3) slightly polluted air with BC levels 50–100 ng m^{-3}, (4) moderately polluted

153   air with BC levels 100–300 ng m^{-3}, (5) polluted air with BC levels 300–1000 ng m^{-3}, and (6) extremely

154   polluted air with BC concentrations > 1000 ng m^{-3} (Figure 1). Previously, BC data were used as indicators

155   for local contamination in Antarctica when BC concentration level exceeded 50 ng m^{-3} (Herenz et al.,

156   2019) or 100 ng m^{-3} (Jang et al., 2018; Kim et al., 2017; Kim et al., 2019; Weller et al., 2011; Weller et

157   al., 2015). Several studies have also reported that BC concentrations not exceeding 15 ng m^{-3} were used

158   to reliably exclude anthropogenically impacted air masses over the Northeast Atlantic (Grigas et al., 2017;

159   O'Dowd et al., 2015; Ovadnevaite et al., 2014).

160   Of the total time period assessed, pristine air conditions represented 30% (mean value of BC: 6.00

161   ± 6.35 ng m^{-3}), clean for 44% (mean value of BC: 29.85 ± 9.81 ng m^{-3}), lightly polluted 19% (mean value

162   of BC: 68.78 ± 13.57 ng m^{-3}), moderately polluted 6% (mean value of BC: 150.43 ± 47.12 ng m^{-3}),

163   polluted 1% (mean value of BC: 498.74 ± 173.87 ng m^{-3}), and extremely polluted less than 1% (mean

164   value of BC: 1537.41 ± 595.47 ng m^{-3}). Together, pristine and clean air conditions accounted for ~72%

165   of the time with the remaining 28% (BC > 50 ng m^{-3}) removed prior to data analysis. For comparison,

166   mean BC measured at the Mace Head Research Station on the Irish coast from 2009–2014 (Grigas et al.,

167   2017) ranged from 8 ng m^{-3} (pristine) to 1700 ng m^{-3} (extreme), where clean and pristine air conditions

168   accounted for 63% of the total time.

169

170   **2.3. Definition of NPF and growth events**

171   NPF events were visually identified by the particle number size distribution based on the protocol

172   described by Dal Maso et al. (2005) and Kulmala et al. (2012). Here, these were defined when a distinct

173   new mode of particles (initially < 25 nm), appearing in the particle number size distribution at nucleation-

174   mode size (3−25 nm), prevailed for more than an hour. Using these criteria, the particle size distribution

175   data showed that in some cases, there was only a short burst of nucleation-mode particles without clearly

176   discernible particle growth, whereas in other cases, particle formation with subsequent particle growth

177   lasted for several hours, representing a regional-scale phenomenon (Ström et al., 2009). This enabled us

178   to determine the particle growth rate (GR), which is not possible during short bursts of nucleation-mode

179   particles.

180   The particle growth and formation rates along with the condensation sink were calculated from the

181   measured particle number size distribution. The GR was determined using the maximum concentration

182   and mode-fitting methods (Dal Maso et al., 2005; Yli-Juuti et al., 2009). GR was calculated by a linear fit

183   through the geometric mean diameter of the nucleation-mode particles as a function of time during NPF.

184   The formation rate (FR) of nucleation-mode particles (J_{3-25}) was calculated by taking into account the

185   time evolution of the particle number concentration in this size range and particle losses due to the

186 coagulation sink and condensational growth out of the size range (Kulmala et al., 2012). The surface area

187 of particles available for the condensation of gaseous molecules can be characterized by a condensation

188 sink (CS), which determines how rapidly vapor molecules condense onto pre-existing particles (Collins

189 et al., 2017; Dal Maso et al., 2002).

190

191 **2.4. Backward trajectory analysis and potential source regions**

192   Air mass back trajectories were obtained using the Hybrid Single-Particle Lagrangian Integrated

193 Trajectory (HYSPLIT) model to investigate their relationships with the physical characteristics of aerosol

194 particles (Draxler and Hess, 1998). The 2 days air mass back trajectories (48 hours) were determined at

195 hourly intervals and combined with satellite-derived geographical information to estimate the transport

196 history of the air masses arriving at the observation site (Jang et al., 2022 and Park et al., 2021). The

197 potential origins of the aerosols were divided into three categories based on the retention time of the 2

198 days back trajectories over three major domains: ocean (including the Weddell and Bellingshausen Seas),

199 sea ice, and land (including the Antarctic Peninsula). Daily geographical information on ocean, sea ice,

200 and land area was obtained from the Sea Ice Index (25 km resolution) provided by the National Snow and

201 Ice Data Center (NSIDC). The sea ice zone was defined as the area with a sea ice coverage >15% (Stroeve

202 et al., 2016). Air masses that passed over the Weddell and Bellingshausen Sea regions were categorized

203 as originating from the ocean (i.e. > 50% retention over the ocean region). The air masses that frequently

204 advected over the sea-ice region were categorized as originated over the sea ice (i.e. > 50% retention over

205 the sea-ice domain). Air masses that traveled through the Antarctic Peninsula were categorized as

206 originating from the land (i.e. > 50% retention over the land). Finally, the air masses which passed over

207 the ocean, sea ice, and land regions simultaneously were categorized as originating from the multiple

208 regions (i.e., 20–40 % retention over each ocean, sea ice, and land domain).

209   To evaluate the influence of oceanic biological characteristics on NPF properties, the phytoplankton

210 biomass of the ocean domains was estimated by calculating their chlorophyll concentration from the

211 Moderate Resolution Imaging Spectroradiometer on the Aqua (MODIS-Aqua) satellite at 4 km resolution

212   during the entire study period. Phytoplankton produces dimethylsulfoniopropionate (DMSP, a precursor

213   of gaseous DMS) and other organic vapors all of which are potential precursors to new particle formation.

214   Thus, the spatiotemporal distribution of sea-surface DMSP could be an indicator of contemporary DMS

215   emissions. The total DMSP concentration on the sea-surface was estimated using the algorithm developed

216   by Galí et al. (2015). The algorithm for the total DMSP concentration was based on the satellite-derived

217   chlorophyll concentration and photosynthetic radiation exposure. To calculate the air mass exposures to

218   ocean chlorophyll and DMSP (Jang et al., 2019), hourly back trajectory position was combined with

219   satellite-derived chlorophyll concentration and total DMSP concentration, providing a good measure for

220   quantitatively investigating the biological exposure history of sampled air over the several days before its

221   arrival at the observation site (Park et al., 2018 and 2021).

222

223   **3. Results and discussion**

224   **3.1. General features and annual cycle**

225   We investigated the overall seasonality of particle number size distributions focusing on NPF events.

226   In addition, local meteorological parameters (e.g., temperature, RH, wind speed, wind direction, pressure,

227   and solar radiation) and air mass back trajectories were used to support the interpretation of the seasonal

228   trends of the particle number size distribution and the dynamics of NPF events observed at the station.

229   **3.1.1. Particle number concentrations and size distributions**

230   Figure 2 and Table 1 shows a time series of the one-hour average total particle number concentration

231   and size-segregated particle number concentrations over the entire measurement period conforming to

232   pristine (BC < 15 ng m^{-3}) and clean (BC: 15–50 ng m^{-3}) conditions. The total particle number

233   concentrations including ultrafine particles (CN$_{2.5}$; TSI 3776 CPC) and particles larger than 10 nm (CN$_{10}$;

234   TSI 3772 TSI) ranged from 60 to 4982 cm^{-3} and 30 to 3304 cm^{-3}, respectively. The annual median number

235   concentrations of particles for the nucleation mode (N$_{NUC}$; 3–25 nm in diameter), Aitken mode (N$_{AIT}$; 25–

236   100 nm in diameter), and accumulation mode (N$_{ACC}$; 100–300 nm in diameter) were 52.4 cm^{-3}, 65.9 cm^{-3}

237   , and 21.7 cm^{-3}, respectively. The highest median N$_{NUC}$, N$_{AIT}$, and N$_{ACC}$ values were recorded in

238   December (193.5 cm^{-3}), December (227.6 cm^{-3}), and January (83.8 cm^{-3}), respectively (Table 1). The

239   lowest N_{NUC}, N_{AIT}, and N_{ACC} values were recorded during austral winter in June – 12.2 cm^{-3}, 12.5 cm^{-3}

240   and 9.2 cm^{-3}, respectively. Overall, clear annual and seasonal patterns of particle number concentrations

241   in all size classes were observed: high concentrations in summer (December–February) and low

242   concentrations in winter (June–August), similar to those observed at Marambio Station in the Antarctic

243   Peninsula (Asmi et al, 2018), at coastal Neumayer Station (Weller et al., 2011), at Concordia Station

244   Dome C (Järvinen et al., 2013), and at Troll Station (Fiebig et al., 2014). Furthermore, the monthly median

245   CN$_{10}$ value was positively correlated with the monthly median N_{NUC} ($R = 0.78$; not shown), implying that

246   the summer maximum of total particle number concentrations was largely influenced by newly formed

247   particles in the Antarctic atmosphere.

248   The meteorological parameters after data filtering (BC < 50 ng m^{-3} indicating pristine and clean

249   conditions) were characterized by a solar radiation range of 0–919 W m^{-2} (median 10.7 W m^{-2}), a

250   temperature range of -20–6 °C (median -1.2 °C), an RH range of 52–98 % (median 88 %), a pressure

251   range of 950–1022 hPa (median 988 hPa), a wind speed range of 0.3–21 m sec^{-1} (median 7.4 m sec^{-1}),

252   and wind direction range of 3–357° (median 296°) (Figure S1). To understand impacts on the particle

253   number size distributions, we determined the relationships between the size-segregated particle number

254   concentrations and meteorological parameters (Figure S2). CN$_{10}$, N_{NUC}, N_{AIT}, and N_{ACC} were positively

255   correlated with both solar radiation intensity and temperature. In particular, N_{NUC} had the highest

256   correlation with solar radiation intensity ($R = 0.39$) of any meteorological condition, suggesting that solar

257   radiation is one of the most important factors influencing NPF events, as it can drive photochemical

258   reactions leading to the production and further reaction of precursor gases. In contrast, there was a weak

259   anticorrelation between RH and N_{NUC}, supporting the view that NPF occurs preferentially at low RH

260   (Dada et al., 2017; Hamed et al., 2011; Jeong et al., 2010; Laaksonen et al., 2008). Field observations

261   have reported that during NPF events, RH was negatively related to the number concentration of freshly

262   formed particles (Jeong et al., 2004; Lachlan-Cope et al., 2020; Weber et al., 1997) because of the

263   enhanced coagulation from scavenging effect of sub-3 nm nanoparticles at high RH and the diminished

264 solar radiation at high RH. Previously, some NPF events were associated with high wind speeds at various

265 Antarctic stations, such as Neumayer (Weller et al., 2015) and Aboa (Asmi et al., 2010; Virkkula et al.,

266 2007). These studies found an enhanced particle number concentration < 10 nm during stormy weather

267 and suggested ion production by frictional processes in fast-moving snow and ice crystals, followed by

268 subsequent ion-mediated nucleation during strong winds. However, in our study, wind speed was not

269 correlated with N_{NUC} ($R = -0.18$), N_{AIT} ($R = -0.04$), or N_{ACC} ($R = -0.05$), as recently suggested by Liu et

270 al. (2018). Our results indicated that wind speed did not affect NPF events. A possible explanation for

271 this wind speed independence is that an increase in wind speed contributes to the enhanced emissions of

272 volatile organic compounds from the surface, but it was also accompanied by cloudy conditions. In

273 summary, the elevated N_{NUC} values (i.e., indicator of NPF events) at King Sejong Station were more

274 likely to be accompanied by high solar radiation, high temperature, and low RH, regardless of wind speed.

275 **3.1.2. Spatial extension of regional nucleation event**

276 NPF events were frequently observed at King Sejong Station, as shown by the size distribution data

277 (Figure 2f). Many previous studies have reported that key steps of the nucleation process (e.g., cluster

278 stabilization) occur in the size range ~2 nm, in line with recent direct observations of atmospheric

279 molecular clusters (Kerminen et al., 2018; Kulmala et al., 2013). However, during NPF events, we did

280 not observe particle formation starting directly from the lower end of the particle size spectrum (2.5 nm),

281 showing that the formation of freshly nucleated particles could not have actually taken place at the site.

282 Indeed, the initial diameter of particles that arrived to the measurement site during the NPF ranged from

283 4 nm to 16 nm (Figure 3a). Median values of NPF event duration (Figure 3b) and growth rate (Figure 3c)

284 were 4.0 hour and 0.83 nm hr^{-1}, respectively. We assumed that they were transported from elsewhere or

285 produced aloft, and detected the appearance of an already grown mode. Consistent with these studies,

286 NPF events can be a regional-scale phenomenon extending over spatial scales of tens to hundreds of

287 kilometers in several regions, such as the remote marine boundary layer (Zheng et al., 2021), Canadian

288 high Arctic (Eureka, Nunavut, on Ellesmere Island in the Canadian Arctic Archipelago) (Tremblay et al.,

289 2019), and Arctic ship-based observations.

290   Assuming the region is characterized by homogenous meteorological conditions, we estimated the

291   spatial scale of NPF by multiplying the time during which a distinct nucleation mode can be observed at

292   the sampling site by the locally measured wind speed (Birmili et al., 2003; Crippa and Pryor, 2013). As

293   shown in Figure 3d, the spatial extend of NPF event associated with substantial particle growth can be

294   16–815 km (median value: 155 km), indicating the large-scale NPF events. Weller et al. (2015) measured

295   size distributions at the coastal Antarctic station Neumayer during two summer campaigns (from 20

296   January to 26 March 2012 and 1 February to 30 April 2014). They found that the spatial extend of NPF

297   event was estimated to be around 170 ± 85 km, taking into account the prevailing wind velocity (around

298   8 ± 4 m s^{-1}) and the confined NPF duration (around 6h).

299

300   **3.1.3. Characteristics of NPF events**

301   NPF events in this study were identified based on the size distribution data measured using the

302   standard-SMPS (Figure 2e) and nano-SMPS (Figure 2f). During the pristine and clean periods

303   (comprising of 355 observation days and 169166 size spectra for the standard-SMPS, and of 349

304   observation days and 165259 size spectra for nano-SMPS), 97 events (26% of observation days) with

305   elevated N_{NUC} were observed when taking place in pristine (BC < 15 ng m^{-3}) and clean (BC: 15–50 ng m^{-3}

306   ^{3}) conditions. Median value of BC concentrations during NPF events was 21.0 ng m^{-3}, similar to that of

307   whole measurement periods after data filtering (median BC value: 18.8 ng m^{-3}) (section 2.2). This

308   indicated that NPF events are independent of occasional increases of BC during clean periods. NPF events

309   were more frequently observed in summer (~55%) than in any other season (Figure 4), with the highest

310   frequency in January (22%) and December (22%) followed by spring (September–November, 34%) and

311   autumn (March–May, 11%). Similar results were reported by Järvinen et al. (2013) based on observations

312   from Dome C and Kim et al. (2019) based on observations from King Sejong Station. Although Järvinen

313   et al. (2013) reported winter events that occurred in the absence of sunlight, we did not detect NPF events

314   during austral winter from May through to August.

315   Air mass back trajectories were calculated at hourly intervals to investigate possible source regions

316   for the observed NPF events. Figure 2g shows the residence times of air masses over the three domains.

317   Based on 2-days air mass transport history analysis, air masses allocated to ocean, sea-ice and land

318   account for 76, 19 and 2%, respectively, during the study period. 97 cases were identified as NPF events,

319   80 of which were observed when the air mass originated over the ocean domain (Figure 4). 12 NPF events

320   were observed in air masses originating over the sea-ice domain, while the remaining 5 events were

321   associated with multi-regional origin (3 cases) and land origin (2 cases). Multi-regional origin indicated

322   air masses simultaneously influenced by all three domains. Our results indicated that NPF events were

323   more common in air masses originating over the ocean and sea ice compared to those originating from

324   the land. Precursors released by both ocean and sea ice could play an important role in the formation of

325   new particles in the Antarctic atmosphere.

326

327   3.2. Case studies

328   This section presents a detailed overview of the marine, sea ice, and multi-regional NPF events.

329   3.2.1. Marine NPF event

330   A striking series of NPF events took place over seven days (Figure 6), starting at approximately

331   00:00 on December 9, 2018. Events starting at midnight can likely indicate their formation few hours

332   earlier during afternoon sunlight, because the events are observed with an already grown nucleation mode.

333   Time series of meteorological parameters, air mass origins, oceanic biological activity (estimated by

334   chlorophyll and DMSP exposures), particle size distribution (measured by nano-SMPS and standard-

335   SMPS), and CCN concentrations are shown in Figure 6. During this time, the prevailing northerly winds

336   (median 307 °) were stable at 7.7 m s^{-1}. Air temperature varied from -1.5 to 2.1 °C (median 0.5 °C) and

337   RH varied from 75–97% (median 89 %). There were no data for solar radiation during these events. Air

338   masses predominantly traveled over the Antarctic Ocean (46.9, 0.7, and 0.4 h over ocean, land, and sea

339   ice, respectively) and could be categorized as originating from the Antarctic Ocean. Specifically, the air

340   mass originated mainly from Bellingshausen Sea (Figure 5a). During this event, the median total DMSP

341   and chlorophyll exposures in the surface sea were 18 nmol L^{-1} and 0.25 mg m^{-3}, respectively.

342   Between 00:00 and 20:00 on December 9, N_{NUC} increased from 196 to 688 cm^{-3}. At the same time,

343   CCN concentrations at 0.4 % supersaturation gradually increased from 138 (00:00 on December 0) to 326

344   cm^{-3} (12:00 on December 11), an increase of 135%. In addition, elevated N_{NUC} occurred at 00:00 on

345   December 13, ranging from 118–522 cm^{-3}. CCN number concentration at 0.4% supersaturation began to

346   increase at this time (95 cm^{-3}) and reached its maximum at 18:00 (503 cm^{-3}), with a concentration increase

347   of 430%.

348

3.2.2. Sea-ice NPF event

350   Two NPF events with subsequent particle growth were detected from around 18:00 on January 2,

351   2018, to around 00:00 on January 3, 2018 (Figure 7). Air temperature and RH during the event were -

352   0.2 °C and 81%, respectively, while solar radiation decreased from 211 to 0.0 W m^{-2}. Winds were mild

353   and stable (2.0–4.5 m sec^{-1}), with a prevailing northwesterly (220–330°) direction and air masses

354   predominantly coming from sea ice. The average retention times of the 2 d back trajectories traveling

355   over ocean, sea ice, and land were 13.1, 30.3, and 4.6 h, respectively, indicating sea-ice-influenced air

356   masses (Figure 5b). Both total DMSP and chlorophyll exposure values suddenly increased from 15:00 to

357   17:00 before the NPF event, while during it, they dropped drastically before somewhat stabilizing, with

358   median exposures of 11.8 nmol L^{-1} and 0.2 mg m^{-3}, respectively.

359   During the event, $CN_{2.5}$ and CN_{10} increased to 3982 and 1534 cm^{-3}, respectively. In addition, the

360   median N_{NUC}, N_{AIT}, and N_{ACC} values were 1148, 286, and 165 cm^{-3}, respectively. Furthermore, elevated

361   CCN concentrations were observed during NPF and growth events. Before the NPF event, CCN

362   concentration at 0.4 % supersaturation was 273.2 cm^{-3} at 17:00 on February 2, then slowly increased to

363   380 cm^{-3}, until 02:00 on February 3. During the NPF event, the CCN concentration increased by 39%.

364

3.2.3. Multiple NPF event

366   An intensive NPF event occurred from November 16 to November 17, 2018 (Figure 8). Air

367   temperature during the event ranged from -2.5 to -0.1 °C (median -1.3 °C). RH ranged from 70–95%

368   (median 79%), slightly lower than that for the marine and sea-ice NPF events described above. During

369   the NPF event observed from 20:00 on November 16 to 02:00 on November 17, solar radiation decreased

370   from 30 to 0 W m^{-2}. This suggested that the NPF event occurred upwind of the measurement site,

371   especially due to observed grown mode. Wind speed ranged from 4.3–9.5 m s^{-1} with a constant direction

372   from the southwest (median 239 °). Air mass back trajectories showed multiple origins before reaching

373   the station, passing over ocean (25.7 h, 53% of residence time), sea ice (12.4 h, 26% of residence time),

374   and land (10.0 h, 21% of residence time) (Figure 5c). During the event, the median total DMSP and

375   chlorophyll exposures in the sea surface were 6.0 nmol L^{-1} and 0.2 mg m^{-3}, respectively.

376   At the start of the event (17:00 on November 16), N_{NUC}, N_{AIT}, and N_{ACC} were 687, 83, and 13 cm^{-3},

377   respectively. The particle number concentration of the nucleation mode sharply increased to 1609 cm^{-3} at

378   the NPF time, and its peak concentration occurred 7 h after the start of the event (00:00 on November 17),

379   indicating spatial extent of the formation region. The peak concentration of Aitken mode particles

380   successively appeared 14 h after the start of the event (07:00 on November 17) and 30 h respectively for

381   accumulation mode particles (23:00 on November 17). The values in the Aitken and accumulation-mode

382   ranges were 91 and 447 cm^{-3}, respectively. We also observed a gradual increase in CCN concentration for

383   23 h. CCN concentration at 0.4 % supersaturation increased from 78 (17:00 on November 16) to 272 cm^{-}

384   ^{3} (23:00 on November 17). This NPF event may have been a source of CCN, which enhanced CCN

385   concentrations by 248%.

386

387   **3.3. Influence of air mass origin on the NPF event**

388   **3.3.1. Parameters related to NPF**

389   Our results show that NPF and its growth events had largely different features depending on air

390   mass origin (Figure S3). Although only 3 cases of multi-regional NPF evets occurred during the pristine

391   and clean periods (not included in Figure 9), the most intense NPF event was observed with multi-regional

392   source region. Here, we compared N_{NUC}, FR GR, and CS, for the ocean and sea ice air masses (Figure 9

393   a-d). The FR, GR, and CS values agreed well with those reported in previous studies at other Antarctic

394   sites (Järv et al., 2013; Kim et al., 2019; Kyrö et al., 2013; Weller et al., 2015). The median N_{NUC} and FR

395   values for the ocean air mass (N_{NUC}: 220 cm^{-3} and FR: 1.2 $\times$ 10^{-2} cm^{-3} s^{-1}) were 1.5 and 2.6 times lower

396   than those of sea ice air mass (N_{NUC}: 343 cm^{-3} and FR: 3.6 $\times$ 10^{-2} cm^{-3} s^{-1}), respectively. This implies

397   that marine NPF events are frequent, but weak in terms of N_{NUC} and FR values. Unlike N_{NUC} and FR,

398   there were no marked differences between the median values of GR and CS by air mass category. The

399   median particle GR values for ocean, sea ice, and multiple air masses were 0.8, 0.7, and 0.9 nm h^{-1},

400   respectively.

401   To examine the effects of oceanic biological activity on NPF properties, we examined solar radiation

402   intensity, chlorophyll exposure, and DMSP exposure for the three air mass (or source region) categories

403   (Figure 9 e-g). There was no difference in the former, while the latter two were highest in air masses

404   originating from the ocean. The median chlorophyll exposure in ocean-influenced air masses (0.2 mg m^{-3}

405   ) was roughly twice that of the sea-ice-influenced air mass (0.1 mg m^{-3}). Total DMSP exposure for the

406   ocean-influenced air mass was ~2.8 times that of the sea-ice air mass.

407

3.3.2. Potential sources facilitating new particle formation

409   Chlorophyll exposure and DMSP exposure were highest during marine NPF events, suggesting a

410   large chance to carry biologically-derived organic compounds from the open ocean areas to the

411   observation site. DMSP, a metabolite of oceanic phytoplankton, is partly converted into gaseous DMS

412   through enzymatic cleavage (Simó, 2001), which is the largest natural sulfur source in the atmosphere

413   (Barnes et al., 2006). Hence, the photooxidation of biogenic DMS in the Antarctic atmosphere (i.e.,

414   secondary DMS-derived aerosols) could be a major contributor to NPF and its growth when the air mass

415   originates from the ocean. Jang at al. (2019) reported that NPF events were more frequent in air masses

416   originating from the Bellingshausen Sea than the Weddell Sea during the biologically productive austral

417   summer, and it is likely that the taxonomic composition of phytoplankton can be related to the formation

418   of new particles in the Antarctic Ocean. Biogenic DMS was found to be a precursor of NPF in coastal

419   Antarctica (Yu and Luo, 2010).

420   Although sea-ice algae bloom underneath the sea-ice cannot be captured by satellite-estimates of

421   biological activity, the air mass exposure to chlorophyll and DMSP for sea-ice NPF events were 2.0 and

422   2.8 times lower than those of marine NPF events. This could be explained by volatile iodine compounds

423   released from ice-covered areas in Antarctica (Jokinen et al; 2018; Saiz-Lopez et al., 2007); however,

424   iodine compounds were not measured during our study period. Previously, iodine compounds were found

425   in large concentrations in and above the sea ice of the Weddell Sea in Antarctica during spring and

426   summer (Atkinson et al., 2012). Roscoe et al. (2015) also confirmed that iodine compounds may

427   contribute to the secondary production of a significant number of particles measured at Halley and

428   Neumayer on the Antarctic coast.

429   In our study, sea-ice NPF events occurred frequently in January (middle of austral summer) and

430   September (early austral spring) (Figure 4). We compared the JR, GR, and CS values for the sea-ice NPF

431   cases observed between January and September (Figure S4) because of their notable differences in ice

432   coverage. In Antarctica, the minimum ice coverage is observed in February and the maximum in

433   September (Parkinson and Cavalieri, 2012). Our results showed that JR, GR, and CS values were much

434   higher in January than in September, indicating different NPF processes. The January events occurred

435   under low ice-coverage conditions, similar to previous studies from polar areas such as Svalbard

436   (Dall'Osto et al., 2017) and Greenland (Dall'Osto et al., 2018). Both studies showed that NPF events are

437   related to biogenic precursors released by open water and melting sea-ice regions, particularly during the

438   summer. In contrast, the September events occurred under high ice-coverage conditions. The monthly

439   median values of solar radiation showed that solar radiation intensity was very low from May to August

440   and then started to increase from September (Table 1). During the September events, median solar

441   radiation intensity was found to be 63 Wm^{-2}. It is therefore possible that elevated sea-ice concentrations

442   under sufficient solar radiation around Antarctica lead to an increase in the concentration of halogen

443   species, resulting in the production of newly formed particles. Solar photooxidation of frozen iodine-

444   containing solution has been shown to accelerate gas-phase iodine concentrations (Kim et al., 2016).

445   The most intensive NPF event was observed in multiple air masses, although the oceanic biological

446   activity was lower than that in the oceanic air mass. This indicated that terrestrial sources from continental

447   Antarctica, in addition to both DMS (mainly from the ocean) and iodine (mainly from sea ice), may have

448   contributed to NPF. First, previous studies have reported that precursors emitted from seabird colonies

449   are linked to NPF (Schmale et al., 2013; Weber et al., 1998). The Chottaebawi area in the southwestern

450   part of King George Island (around 2 km away from our observation site) is an important penguin colony

451   in the Antarctic region (Lee et al., 2009), while the cape area near King Sejong Station is abundantly

452   populated by flying seabirds such as skua. Given the proximity and abundance of seabird colonies at King

453   Sejong Station, seabird colony emissions are the likely sources of NPF. Second, biogenic emissions from

454   vegetation in the Antarctic Peninsula, mainly composed of relatively small and sparse patches of lichens

455   and mosses (Miranda et al., 2020), could be associated with NPF and growth. Kim et al. (2006) studied

456   plant communities on the Barton Peninsula around King Sejong Station in the maritime Antarctic and

457   concluded that ~47% of the investigated area was covered by vegetation although generally sparse. Finally,

458   biogenic precursors from meltwater ponds in continental Antarctica have also been suggested (Kyrö et

459   al., 2013) as a possible source of aerosol production (Weller et al., 2018). Overall, our data suggest that

460   complex interconnected ecosystems across ocean, sea ice, and land can lead to an enhancement in

461   Antarctic NPF.

3.3.3. NPF as a source of CCN

463   For a given SS of 0.4%, the median CCN number concentrations were rather similar 184, 144, and

464   178 cm^{-3} for ocean, sea ice, and multiple air masses, respectively (Figure 9h). Of the 83 NPF events, CCN

465   concentrations increased by 2–268% (median 44%) following 1 to 36 hours (median 8 hours) after NPF

466   events. The median increase in CCN concentrations was 44 %, 34 %, and 107 % for ocean, sea ice, and

467   multiple air masses, respectively. NPF can be an important source of CCN in Antarctica, and the highest

468   CCN enhancement was observed when air masses passed through multiple regions, followed by ocean

469   and sea-ice regions. Moreover, we newly calculated CCN increase rate, which defined as the change rates

470   of representative CCN concentrations ($CCN_1(t_1)$ and $CCN_2(t_2)$) with the highest CCN concentrations at

471   certain times (t_1 and t_2), when elevated CCN concentration was observed during the NPF. The CCN rate

472   varied from 1.4 to 76.7 cm^{-3} hr^{-1}, with a median value of 10.2 cm^{-3} hr^{-1}. Our results provide the first direct

473   evidence of CCN production resulting from an NPF event in the Antarctic atmosphere, based on

474   simultaneous measurements of particle number size distribution (e.g., diameter ranges of 2.5–300 nm)

475   and CCN number concentrations in real time throughout the year.

476   We also compared CCN activity and critical diameter for the three selected periods (Figure 9i and

477   j). The median values of CCN activity, i.e. the ratio of the number concentration of particles that activated

478   to become CCN at a given supersaturation to the total number concentration or particles larger than 10

479   nm (CN$_{10}$), were similar (about 5%) in three different air masses. The critical diameter (D_c), the diameter

480   at which the integration of aerosol size distribution from the largest particle diameter to the lowest one

481   matches the measured CCN concentration, was determined using the measured aerosol size distribution,

482   CN$_{10}$, and CCN concentrations (Furutani et al., 2018). The median D_c value at 0.4% supersaturation was

483   estimated to be 41 nm, 32 nm, and 37 nm for ocean, sea ice, and multiple air masses, respectively. These

484   results agreed well with those reported in previous studies that determined D_c at the Finnish Antarctic

485   Research Station, Aboa (Kyrö et al., 2013), a clean subarctic background site (Komppula et al., 2005),

486   and over remote Southern Ocean around Antarctica (Fossum et al., 2018; Fossum et al., 2020). For

487   instance, Kyrö et al. (2013) found the smallest D_c at 48 nm. The median D_c, as suggested by Komppula

488   et al. (2005), varied from 50–128 nm (average 80 nm). The D_c value for maritime polar and marine

489   modified continental Antarctic air masses were 71 and 59 nm, respectively (Fossum et al., 2020).

490

491   **4. Conclusions**

492   We measured the number size distribution of 2.5–300 nm particles and CCN number concentrations

493   at King Sejong Station in the Antarctic Peninsula continuously from January 1 to December 31, 2018.

494   The annual median values of N$_{NUC}$, N$_{AIT}$, and N$_{ACC}$ were 52.4 cm^{-3}, 65.9 cm^{-3}, and 21.7 cm^{-3}, respectively.

495   Overall, clear annual and seasonal patterns of particle number concentrations in all size classes were

496   observed (high concentrations in summer and low concentrations in winter). Furthermore, the monthly

497   CN_{10} value was positively correlated with the monthly N_{NUC}, implying that summer maximum particle

498   concentrations could be largely influenced by newly formed particles in the Antarctic atmosphere. Among

499   meteorological parameters, the elevated N_{NUC} values (i.e., indicators of NPF events) were more likely to

500   be accompanied by high solar radiation, high temperature, and low RH, regardless of wind speed.

501   NPF events were identified based on size distribution data measured using two SMPSs. During the

502   pristine and clean periods, 97 events (26% of observation days) with elevated N_{NUC} were observed. NPF

503   events occurred more frequently in summer than in any other season. Based on air mass back-trajectory

504   analysis, we distinguished three different types of NPF events: marine (80 cases), sea ice (12 cases), and

505   multiple (3 cases). Marine NPF events were frequent and weak (N_{NUC}, 220 cm^{-3}; FR = 1.2 × 10^{-2} cm^{-3} s^{-1}

506   ; GR = 0.8 nm hr^{-1}) and occurred when the air mass exposure to oceanic   phytoplankton was high

507   (chlorophyll, 0.2 mg m^{-3}; DMSP, 18 nmol L^{-1}). The photooxidation of biogenic DMS in the Antarctic

508   atmosphere could be a major contributor to marine NPF events. In contrast, sea-ice NPF events (N_{NUC},

509   343 cm^{-3}; FR, 3.6 × 10^{-2} cm^{-3} s^{-1}; GR, 0.7 nm h^{-1}) were observed when the air mass exposure to oceanic

510   phytoplankton was relatively low (chlorophyll, 0.1 mg m^{-3}; DMSP, 7 nmol L^{-1}), which may be due to

511   volatile iodine compounds released from ice-covered areas. Strong NPF events (N_{NUC}, 516 cm^{-3}; FR, 3.2

512   × 10^{-2} cm^{-3} s^{-1}; GR, 0.9 nm hr^{-1}) were associated with multiple air masses, indicating complex

513   interconnected ecosystems leading to an enhancement in Antarctic NPF.

514   To investigate the connection between newly formed particles and CCN production, we compared

515   CCN properties for the three air mass categories. The median CCN number concentrations at a given SS

516   of 0.4% were 184, 144, and 178 cm^{-3} for ocean, sea ice, and multiple air masses, respectively. Of the 83

517   events, an increase in CCN concentrations after the NPF events was detected, ranging from 2–268 %

518   (median 44 %). The median increase in CCN concentrations was 44 %, 34 %, and 107 % for ocean, sea

519   ice, and multiple air masses, respectively. NPF events led to increased CCN concentrations at King Sejong

520   Station. The median value of D_c at a supersaturation of 0.4% was estimated to be 41 nm, 32 nm, and 37

521   nm for ocean, sea ice, and multiple air masses, respectively. This study is the first to report CCN

522   production resulting from NPF events in the Antarctic atmosphere in the Antarctic Peninsula. However,

523   further detailed measurements of the chemical properties of aerosol particles and precursors during NPF

524   events are required to better understand the contribution of these compounds to the formation and growth

525   of aerosol particles and to explore their impacts on CCN formation in the remote Antarctic environment.

526

527   **Data availability**

528   The data analyzed in this publication will be readily provided upon request to the corresponding author

529   (yjyoon@kopri.re.kr).

530

531   **Author contributions**

532   JP and YJY designed the study. JP, HK, YG, EJ, K-TP, SP, and YJY analyzed data. JP wrote the

533   manuscript. CHJ, DC, and CO'D all commented on and discussed the manuscript.

534

535   **Competing interests**

536   The authors declare that they have no conflict of interest.

537

538   **Acknowledgments**

539   We would like to thank the many technicians and scientists of the overwintering crews. This work was

540   supported by the KOPRI project (PE23030).

541

542   **References**

543   Asmi, E., Frey, A., Virkkula, A., Ehn, M., Manninen, H. E., Timonen, H., Tolonen-Kivimäki, O., Aurela,
544   M., Hillamo, R., and Kulmala, M.: Hygroscopicity and chemical composition of Antarctic sub-
545   micrometre aerosol particles and observations of new particle formation, Atmos. Chem. Phys., 10,
546   4253–4271, https://doi.org/10.5194/acp-10-4253-2010, 2010.
547   Asmi, E., Neitola, K., Teinila, K., Rodriguez, E., Virkkula, A., Backman, J., Bloss, M., Jokela, J.,
548   Lihavainen, H., De Leeuw, G., Paatero, J., Aaltonen, V., Mei, M., Gambarte, G., Copes, G., Albertini,
549   M., Fogwill, G. P., Ferrara, J., Barlasina, M. E., and Sanchez, R.: Primary sources control the
550   variability of aerosol optical properties in the Antarctic Peninsula, Tellus B, 70, 1,
551   https://doi.org/10.1080/16000889.2017.1414571, 2018.
552   Atkinson, H. M., R.-J. Huang, R. Chance, H. K. Roscoe, C. Hughes, B.avison, A. Schönhardt, A. S.
553   Mahajan, A. Saiz-Lopez, and P. S. Liss (2012), Iodine emissions from the sea ice of the Weddell
554   Sea, Atmos. Chem. Phys., 12, 11,229–11,244, doi:10.5194/acp-12-11229-2012.
555   Barnes, I., Hjorth, J., and Mihalopoulos, N.: Dimethyl sulfide and dimethyl sulfoxide and their oxidation
556   in the atmosphere, Chem. Rev., 106, 940–975, 2006.
557   Belosi, F., Contini, D., Donateo, A., Santachiara, G., and Prodi, F.: Aerosol size distribution at Nansen Ice
558   Sheet Antarctica, Atmos. Res., 107, 42–50, 2012.

559   Birmili, W., Berresheim, H., Plass-Dülmer, C., Elste, T., Gilge, S., Wiedensohler, A., and Uhrner, U.: The
560   Hohenpeissenberg aerosol formation experiment (HAFEX): a long-term study including size-
561   resolved aerosol, H_2SO_4, OH, and monoterpenes measurements, Atmos. Chem. Phys., 3, 361–376,
562   https://doi.org/10.5194/acp-3-361-2003, 2003

563   Buenrostro Mazon S., Kontkanen J., Manninen H.E., Nieminen T., Kerminen V.-K. & Kulmala M. 2016:
564   A long-term comparison of nighttime cluster events and daytime ion formation in a boreal forest.
565   Boreal Env. Res. 21: 242–261.

566   Carslaw, K. S., Lee, L. A., Reddington, C. L., Pringle, K. J., Rap, A., Forster, P. M., Mann, G. W.,
567   Spracklen, D. V., Woodhouse, M. T., Regayre, L. A., and Pierce, J. R.: Large contribution of natural
568   aerosols to uncertainty in indirect forcing, Nature, 503, 67–71, doi:10.1038/nature12674, 2013.

569   Chen, J. L., Wilson, C. R., Blankenship, D., and Tapley, B. D.: Accelerated Antarctic ice loss from satellite
570   gravity measurements, Nat. Geosci., 2, 859–862, 2009.

571   Chen, D. R., Pui, D. Y. H., Hummes, D., Fissan, H., Quant, F. R., and Sem, G. J.: Design and evaluation
572   of a nanometer aerosol differential mobility analyzer (Nano-DMA), J. Aerosol. Sci., 29, 497–509,
573   doi:10.1016/S0021-8502(97)10018-0, 1998.

574   Collins, D. B., Burkart, J., Chang, R. Y.-W., Lizotte, M., Boivin-Rioux, A., Blais, M., Mungall, E. L.,
575   Boyer, M., Irish, V.E., Massé, G., Kunkel, D., Tremblay, J.-É., Papakyriakou, T., Bertram, A. K.,
576   Bozem, H., Gosselin, M., Levasseur, M., and Abbatt, J. P. D.: Frequent ultrafine particle formation
577   and growth in Canadian Arctic marine and coastal environments, Atmos. Chem. Phys., 17, 13119–
578   13138, https://doi.org/10.5194/acp-17-13119-2017, 2017.

579   Crippa, P. and Pryor, S. C.: Spatial and temporal scales of new particle formation events in eastern North
580   America, Atmos. Environ., 75, 257–264, https://doi.org/10.1016/j.atmosenv.2013.04.051, 2013

581   Dada, L., Paasonen, P., Nieminen, T., Buenrostro Mazon, S., Kontkanen, J., Peräkylä, O., Lehtipalo, K.,
582   Hussein, T., Petäjä, T., Kerminen, V. M., Bäck, J., and Kulmala, M.: Long-term analysis of clear-
583   sky new particle formation events and nonevents in Hyytiälä, Atmos. Chem. Phys., 17(10), 6227–
584   6241, doi:10.5194/acp-17-6227-2017, 2017.

585   Dall'Osto, M., Ovadnevaite, J., Paglione, M., Beddows, D. C. S., Ceburnis, D., Cree, C., Cortes, P.,
586   Zamanillo, M., Nunes, S. O., Perez, G. L., Ortega-Retuerta, E., Emelianov, M., Vaque, D., Marrase,
587   C., Estrada, M., Sala, M. M., Vidal, M., Fitzsimons, M. F., Beale, R., Airs, R., Rinaldi, M., Decesari,
588   S., Facchini, M. C., Harrison, R. M., O'Dowd, C., and Simo, R.: Antarctic sea ice region as a source
589   of biogenic organic nitrogen in aerosols, Sci. Rep., 7, 6047, https://doi.org/10.1038/s41598-017-
590   06188-x, 2017.

591   Dall'Osto, M., Beddows, D. C. S., Tunved, P., Krejci, R., Ström,J., Hansson, H.-C., Yoon, Y. J., Park, K.-
592   T., Becagli, S., Udisti, R., Onasch, T., O'Dowd, C. D., Simó, R., and Harrison, R. M.: Arctic sea ice
593   melt   leads   to   atmospheric   new   particle   formation,   Sci.   Rep.,   7,   3318,
594   https://doi.org/10.1038/s41598-017-03328-1, 2017.

595   Dall'Osto, M., Geels, C., Beddows, D. C. S., Boertmann, D., Lange, R., Nøjgaard, J. K., Harrison Roy,
596   M., Simo, R., Skov, H., and Massling, A.: Regions of open water and melting sea ice drive new
597   particle formation in North East Greenland, Sci. Rep., 8, 6109, https://doi.org/10.1038/s41598-018-
598   24426-8, 2018.

599   Dal Maso, M.: Condensation and coagulation sinks and formation of nucleation mode particles in coastal
600   and   boreal   forest   boundary   layers,   J.   Geophys.   Res.,   107,   8097,
601   https://doi.org/10.1029/2001jd001053, 2002

602   Dal Maso, M., Kulmala, M., Riipinen, I., Wagner, R., Hussein T., Aalto, P. P., and Lehtinen, K. E. J.:
603   Formation and growth of fresh atmospheric aerosols: eight years of aerosol size distribution data
604   from SMEAR II, Hyytiälä, Finland, Boreal Environ. Res., 10, 323–336, 2005.

605   Draxler, R. R. and Hess, G. D.: An overview of the HYSPLIT_4modelling system for trajectories, Aust.
606   Meteorol. Mag., 47, 295–308, 1998.

607   Ehn, M., Vuollekoski, H., Petäjä, T., Kerminen, V.-M., Vana, M., Aalto, P., de Leeuw, G., Ceburnis, D.,
608   Dupuy, R., O'Dowd, C. D., and Kulmala, M.: Growth rates during coastal and marine new particle
609   formation   in   western   Ireland,   J.   Geophys.   Res.-Atmos.,   115,   D18218,

610   https://doi.org/10.1029/2010JD014292, 2010.
611   Fiebig, M., Hirdman, D., Lunder, C. R., Ogren, J. A., Solberg, S., Stohl, A., and Thompson, R. L.: Annual
612   cycle of Antarctic baseline aerosol: controlled by photooxidation-limited aerosol formation, Atmos.
613   Chem. Phys., 14, 3083–3093, https://doi.org/10.5194/acp-14-3083-2014, 2014.
614   Fossum, K. N., Ovadnevaite, J., Ceburnis, D., Dall'Osto, M., Marullo, S., Bellacicco, M., Simó, R., Liu,
615   D., Flynn, M., Zuend, A., and O'Dowd, C.: Summertime primary and secondary contributions to
616   Southern Ocean cloud condensation nuclei, Sci. Rep., 8, 13844, https://doi.org/10.1038/s41598-
617   018-32047-4, 2018.
618   Fossum, K. N., Ovadnevaite, J., Ceburnis, D., Preißler, J., Snider, J. R., Huang, R. -J., Zuend, A., and
619   O'Dowd, C.: Sea-spray regulates sulfate cloud droplet activation over oceans, npj Clim. Atmos.
620   Sci., 3, 14, https://doi.org/10.1038/s41612-020-0116-2, 2020.
621   Furutani, H., Dall'osto, M., Roberts, G. C., and Prather, K. A.: Assessment of the relative importance of
622   atmospheric aging on CCN activity derived from field observations, Atmos. Environ., 42, 3130–
623   3142, 2008.
624   Galí, M., Devred, E., Levasseur, M., Royer, S.-J., and Babin, M.: A remote sensing algorithm for
625   planktonic dimethylsulfoniopropionate (an analysis of global patterns, Remote Sens. Environ., 171,
626   171–184, https://doi.org/10.1016/j.rse.2015.10.012, 2015.
627   Giordano, M. R., Kalnajs, L. E., Avery, A., Goetz, J. D., Davis, S. M., and DeCarlo, P. F.: A missing source
628   of aerosols in Antarctica – beyond long-range transport, phytoplankton, and photochemistry, Atmos.
629   Chem. Phys., 17, 1–20, https://doi.org/10.5194/acp-17-1-2017, 2017
630   Giordano, M. R., Kalnajs, L. E., Goetz, J. D., Avery, A. M., Katz, E., May, N. W., Leemon, A., Mattson,
631   C., Pratt, K. A., and DeCarlo, P. F.: The importance of blowing snow to halogencontaining aerosol
632   in coastal Antarctica: influence of source region versus wind speed, Atmos. Chem. Phys., 18,
633   16689–16711, https://doi.org/10.5194/acp-18-16689-2018, 2018.
634   Gras, J. L. and Keywood, M.: Cloud condensation nuclei over the Southern Ocean: wind dependence and
635   seasonal cycles, Atmos. Chem. Phys., 17, 4419–4432, https://doi.org/10.5194/acp-17-4419-2017,
636   2017.
637   Grigas, T., Ovadnevaite, J., Ceburnis, D., Moran, E., McGovern, F. M., Jennings, S. G., and O'Dowd, C.:
638   Sophisticated clean air strategies required to mitigate against particulate organic pollution, Sci. Rep.,
639   7, 44737, https://doi.org/10.1038/srep44737, 2017.
640   Hamed, A., Korhonen, H., Sihto, S.-L., Joutsensaari, J., Jarvinen, H., Petaja, T., Arnold, F., Nieminen, T.,
641   Kulmala, M., Smith, J. N., Lehtinen, K. E. J., and Laaksonen, A.: The role of relative humidity in
642   continental   new   particle   formation,   J.   Geophys.   Res.,   116,   D03202,
643   https://doi.org/10.1029/2010JD014186, 2011.
644   Hara, K., Osada, K., Nishita-Hara, C., and Yamanouchi, T.: Seasonal variations and vertical features of
645   aerosol particles in the Antarctic troposphere, Atmos. Chem. Phys., 11, 5471–5484,
646   https://doi.org/10.5194/acp-11-5471-2011, 2011.
647   Herenz, P., Wex, H., Mangold, A., Laffineur, Q., Gorodetskaya, I. V., Fleming, Z. L., Panagi, M., and
648   Stratmann, F.: CCN measurements at the Princess Elisabeth Antarctica research station during three
649   austral summers, Atmos. Chem. Phys., 19, 275–294, https://doi.org/10.5194/acp-19-275-2019,
650   2019.
651   Humphries, R. S., Schofield, R., Keywood, M. D., Ward, J., Pierce, J. R., Gionfriddo, C. M., Tate, M. T.,
652   Krabbenhoft, D. P., Galbally, I. E., Molloy, S. B., Klekociuk, A. R., Johnston, P. V., Kreher, K.,
653   Thomas, A. J., Robinson, A. D., Harris, N. R. P., Johnson, R., and Wilson, S. R.: Boundary layer
654   new particle formation over East Antarctic sea ice – possible Hg-driven nucleation?, Atmos. Chem.
655   Phys., 15, 13339–13364, https://doi.org/10.5194/acp-15-13339-2015, 2015.
656   Humphries, R. S., Klekociuk, A. R., Schofield, R., Keywood, M., Ward, J., and Wilson, S. R.:
657   Unexpectedly high ultrafine aerosol concentrations above East Antarctic sea ice, Atmos. Chem.
658   Phys., 16, 2185–2206, https://doi.org/10.5194/acp-16-2185-2016, 2016.
659   IPCC: Climate change 2013: The physical science basis, Intergovernmental panel on Climate Change,
660   Cambridge University Press, New York, USA, 571–740, 2013.

Ito, T.: Size distribution of Antarctic submicron aerosols, Tellus B, 45, 145–59, 1993.

Jang, E., Park, K.-T., Yoon, Y. J., Kim, T.-W., Hong, S.-B., Becagli, S., raversi, R., Kim, J., and Gim, Y.: New particle formation events observed at the King Sejong Station, Antarctic Peninsula – Part 2: Link with the oceanic biological activities, Atmos. Chem. Phys., 19, 7595–7608, https://doi.org/10.5194/acp-19-7595-2019, 2019.

Jang, E., Park, K.-T., Yoon, Y.J., Kim, K., Gim, Y., Chung, H.Y., Lee, K., Choi, J., Park, J., Park, S.-J., Koo, J.-H., Fernandez, R.P., and Saiz-Lopez, A.: First-year sea ice leads to an increase in dimethyl sulfide-induced particle formation in the Antarctic Peninsula, Sci. Total Environ., 803, 150002. https://doi.org/10.1016/j.scitotenv.2021.150002, 2022.

Jeong, C. H., Hopke, P. K., Chalupa, D. . and Utell, M. : Characteristics of nucleation and growth events of ultrafine particles measured in Rochester, N.Y., Environ. Sci. Technol., 38, 1933–1940, 2004.

Jeong, C.-H. H., Evans, G. J., McGuire, M. L., Y.-W. Chang, R., Abbatt, J. P. D. D., Zeromskiene, K., Mozurkewich, M., Li, S.-M. M., Leaitch, W. R., Chang, R. Y.-W., Abbatt, J. P. D. D., Zeromskiene, K., Mozurkewich, M., Li, S.-M. M. and Leaitch, W. R.: Particle formation and growth at five rural and urban sites, Atmos. Chem. Phys., 10(16), 7979–7995, doi:10.5194/acp-10-7979-2010, 2010.

Järvinen, E., Virkkula, A., Nieminen, T., Aalto, P. P., Asmi, E., Lanconelli, C., Busetto, M., Lupi, A., Schioppo, R., Vitale, V., Mazzola, M., Petäjä, T., Kerminen, V.-M., and Kulmala, M.: Seasonal cycle and modal structure of particle number size distribution at Dome C, Antarctica, Atmos. Chem. Phys., 13, 7473–7487, https://doi.org/10.5194/acp-13-7473-2013, 2013.

Jokinen, T., Sipilä, M., Kontkanen, J., Vakkari, V., Tisler, P., Duplissy, E.-M., Junninen, H., Kangasluoma, J., Manninen, H. E., Petäjä, T., Kulmala, M.,Worsnop, D. R., Kirkby, J., Virkkula, A., and Kerminen, V.-M.: Ion-induced sulfuric acid–ammonia nucleation drives particle formation in coastal Antarctica, Sci. Adv., 4, eaat9744, https://doi.org/10.1126/sciadv.aat9744, 2018.

Kerminen, V.-M., Chen, X., Vakkari, V., Petäjä, T., Kulmala, M., and Bianchi, F.: Atmospheric new particle formation and growth: review of field observations, Environ. Res. Lett., 13, 103003, https://doi.org/10.1088/1748-9326/aadf3c, 2018.

Kim, J., Yoon, Y. J., Gim, Y., Kang, H. J., Choi, J. H., Park, K.-T., and Lee, B. Y.: Seasonal variations in physical characteristics of aerosol particles at the King Sejong Station, Antarctic Peninsula, Atmos. Chem. Phys., 17, 12985–12999, https://doi.org/ 10.5194/acp- 17-12985-2017, 2017.

Kim, J., Yoon, Y. J., Gim, Y., Choi, J. H., Kang, H. J., Park, K.-T., Park, J., and Lee, B. Y.: New particle formation events observed at King Sejong Station, Antarctic Peninsula – Part 1: Physical characteristics and contribution to cloud condensation nuclei, Atmos. Chem. Phys., 19, 7583–7594, https://doi.org/10.5194/acp-19-7583-2019, 2019.

Kim, J. H., Ahn, I. -Y., Lee, K. S., Chung, H., and Choi, H.-G.: Vegetation of Barton Peninsula in the neighbourhood of King Sejong Station (King George Island, maritime Antarctic), Polar, Biol., 30, 903–916, https://doi.org/10.1007/s00300-006-0250-2, 2007.

Kim, K., Yabushita, A., Okumura, M., Saiz-Lopez, A., Cuevas, C. A., Blaszczak-Boxe, C. S., Min, D. W., Yoon, H.-I., and Choi, W.: Production of Molecular Iodine and Tri-iodide in the Frozen Solution of Iodide: Implication for Polar Atmosphere, Environ. Sci. Technol., 50, 1280–1287, 2016.

Komppula, M., Lihavainen, H., Kerminen, V.-M., Kulmala, M., and Viisanen, Y.: Measurements of cloud droplet activation of aerosol particles at a clean subarctic background site, J. Geophys. Res., 110, D06204, doi:10.1029/2004JD005200, 2005.

Kulmala, M., Vehkamäki, H., Petäjä, T., Dal Maso, M., Lauri, A., Kerminen, V. M., Birmili, W., and McMurry, P. H.: Formation and growth rates of ultrafine atmospheric particles: a review of observations, J. Aerosol Sci., 35, 143–176, https://doi.org/10.1016/j.jaerosci.2003.10.003, 2004.

Kulmala, M., Petäjä, T., Nieminen, T., Sipilä, M., Manninen, H. E., Lehtipalo, K., Dal Maso, M., Aalto, P. P., Junninen, H., Paasonen, P., Riipinen, I., Lehtinen, K. E. J., Laaksonen, A., and Kerminen, V.-M.: Measurement of the nucleation of atmospheric aerosol particles, Nat. Protoc., 7, 1651–1667, 2012.

Kulmala, M., Kontkanen, J., Junninen, H., Lehtipalo, K., Manninen, H. E. Nieminen, T., Petäjä, T., Sipilä,

712   M., Schobesberger, S., Rantala, P., Franchin, A., Jokinen, T., Järvinen, E., Äijälä, M., Kangasluoma,
713   J., Hakala, J., Aalto, P. P., Paasonen, P., Mikkilä, J., Vanhanen, J., Aalto, J., Hakola, H., Makkonen,
714   U., Ruuskanen, T., Mauldin III, R. L., Duplissy, J., Vehkamäki, H., Bäck, J., Kortelainen, A.,
715   Riipinen, I., Kurtén, T., Johnston, M. V., Smith,

716 Kyrö, E.-M., Kerminen, V.-M., Virkkula, A., Dal Maso, M., Parshintsev, J., Ruíz-Jimenez, J., Forsström,
717   L., Manninen, H. E., Riekkola, M.-L., Heinonen, P., and Kulmala, M.: Antarctic new particle
718   formation from continental biogenic precursors, Atmos. Chem. Phys., 13, 3527–3546,
719   https://doi.org/10.5194/acp-13-3527-2013, 2013.

720 Laaksonen, A., Kulmala, M., O'Dowd, C. D., Joutsensaari, J., Vaattovaara, P., Mikkonen, S., Lehtinen,
721   K. E. J., Sogacheva, L., Dal Maso, M., Aalto, P., Petäjä, T., Sogachev, A., Yoon, Y. J., Lihavainen,
722   H., Nilsson, D., Facchini, M. C., Cavalli, F., Fuzzi, S., Hoffmann, T., Arnold, F., Hanke, M., Sellegri,
723   K., Umann, B., Junkermann, W., Coe, H., Allan, J. D., Alfarra, M. R., Worsnop, D. R., Riekkola,
724   M.-L., Hyötyläinen, T., and Viisanen, Y.: The role of VOC oxidation products in continental new
725   particle formation, Atmos. Chem. Phys., 8, 2657–2665, https://doi.org/10.5194/acp-8-2657-2008,
726   2008.

727 Lachlan-Cope, T., Beddows, D. C. S., Brough, N., Jones, A. E., Harrison, R. M., Lupi, A., Yoon, Y. J.,
728   Virkkula, A., and Dall'Osto, M.: On the annual variability of Antarctic aerosol size distributions at
729   Halley Research Station, Atmos. Chem. Phys., 20, 4461–4476, https://doi.org/10.5194/acp-20-
730   4461-2020, 2020.

731 Lee, Y. I., Lim, H. S., and Yoon, H. I.: Carbon and nitrogen isotope composition of vegetation on King
732   George Island, maritime Antarctic, Polar Biol. 32, 1607–1615). https://doi.org/10.1007/s00300-
733   009-0659-5, 2009.

734 Liu, J., Dedrick, J., Russell, L. M., Senum, G. I., Uin, J., Kuang, C., Springston, S. R., Leaitch, W. R.,
735   Aiken, A. C., and Lubin, D.: High summertime aerosol organic functional group concentrations
736   from marine and seabird sources at Ross Island, Antarctica, during AWARE, Atmos. Chem. Phys.,
737   18, 8571–8587, https://doi.org/10.5194/acp-18-8571-2018, 2018.

738 Miranda, V., Pina, P., Heleno, S., Vieira, G., Mora, C., and Schaefer, C.E.: Monitoring recent changes of
739   vegetation in Fildes Peninsula (King George Island, Antarctica) through satellite imagery guided by
740   UAV surveys. Sci. Total Environ. 704, 135295. https://doi.org/10.1016/j.scitotenv.2019.135295,
741   2020.

742 O'Dowd, C. D.: On the spatial extent and evolution of coastal aerosol plumes, J. Geophys. Res.-Atmos,
743   107, 8105, doi:8110.1029/2001JD000 422, 2002

744 O'Dowd, C., Ceburnis, D., Ovadnevaite, J., Bialek, J., Stengel, D. B., Zacharias, M., Nitschke, U., Connan,
745   S., Rinaldi, M., Fuzzi, S., Decesari, S., Cristina Facchini, M., Marullo, S., Santoleri, R., Dell'Anno,
746   A., Corinaldesi, C., Tangherlini, M., and Danovaro, R.: Connecting marine productivity to sea-spray
747   via nanoscale biological processes: Phytoplankton Dance or Death Disco?, Sci. Rep., 5, 14883,
748   doi:10.1038/srep14883, 2015.

749 O'Dowd, C. D, Lowe, J. A., Smith, M. H., Davison, B., Hewitt, C. N., and Harrison, R. M.: Biogenic
750   sulphur emissions and inferred non-sea-salt-sulphate cloud condensation nuclei in and around
751   Antarctica, J. Geophys. Res.-Atmos. 102, 12839–12854, 1997.

752 Ovadnevaite, J., Ceburnis, D., Leinert, S., Dall'Osto, M., Canagaratna, M., O'Doherty, S., Berresheim,
753   H., and O'Dowd, C.: Submicron NE Atlantic marine aerosol chemical composition and abundance:
754   Seasonal trends and air mass categorization, J. Geophys. Res.-Atmos., 119, 11850–11863,
755   doi:10.1002/2013jd021330, 2014.

756 Pant, V., Siingh, D., and Kamra, A. K.: Size distribution of atmospheric aerosols at Maitri, Antarctica,
757   Atmos. Environ., 45, 5138–5149, 2011.

758 Park, J., Dall'Osto, M., Park, K., Gim, Y., Kang, H. J., Jang, E., Park, K.-T., Park, M., Yum, S. S., Jung,
759   J., Lee, B. Y., and Yoon, Y. J.: Shipborne observations reveal contrasting Arctic marine, Arctic
760   terrestrial and Pacific marine aerosol properties, Atmos. Chem. Phys., 20, 5573–5590,
761   https://doi.org/10.5194/acp-20-5573-2020, 2020.

762 Park, K. T. Lee, K. Kim, T. W. Yoon, Y. J. Jang, E. H. Jang, S. Lee, B. Y.and Hermansen, O.:

763   Atmospheric DMS in the Arctic Ocean and its relation to phytoplankton biomass, Global
764   Biogeochem. Cy., 32, 351–359, https://doi.org/10.1002/2017GB005805, 2018.

765 Park, K.-T., Yoon, Y.J., Lee, K., Tunved, P., Krejci, R., Ström, J., Jang, E., Kang, H.J., Jang, S., Park, J.,
766   Lee, B.Y., Traversi, R., Becagli, S., and Hermansen, O.: Dimethyl Sulfide-Induced Increase in
767   Cloud Condensation Nuclei in the Arctic Atmosphere, Global Biogeochem. Cy., 35,
768   e2021GB006969, https://doi.org/10.1029/2021GB006969, 2021.

769 Parkinson, C. L. and Cavalieri, D. J.: Antarctic sea ice variability and trends, 1979–2010, The Cryosphere,
770   6, 871–880, https://doi.org/10.5194/tc-6-871-2012, 2012.

771 Pritchard, H. D., Arthern, R. J., Vaughan, D. G., and Edwards, L. A.: Extensive dynamic thinning on the
772   margins of the Greenland and Antarctic ice sheets, Nature, 461, 971–975, 2009.

773 Pushpawela, B., Jayaratne, R., and Morawska, L.: The influence of wind speed on new particle formation
774   events in an urban environment, Atmos. Res. 215, 37–41, 2019.

775 Roscoe, H. K., Jones, A. E., Brough, N., Weller, R., Saiz-Lopez, A., Mahajan, A. S., Schoenhardt, A.,
776   Burrows, J.P., and Fleming, Z. L.: Particles and iodine compounds in coastal Antarctica, J. Geophys.
777   Res.-Atmos.,120, 7144–7156, https://doi.org/10.1002/2015JD023301, 2015.

778 Saiz-Lopez, A., Mahajan, A. S., Salmon, R. A., Bauguitte, S. J. B., Jones, A. E., Roscoe, H. K., and Plane,
779   J. M. C.: Boundary layer halogens in coastal Antarctica, Science, 317, 348–351,
780   doi:10.1126/science.1141408, 2007

781 Schmale, J., Schneider, J., Nemitz, E., Tang, Y. S., Dragosits, U., Blackall, T. D., Trathan, P. N., Phillips,
782   G. J., Sutton, M., and Braban, C. F.: Sub-Antarctic marine aerosol: dominant contributions from
783   biogenic sources, Atmos. Chem. Phys., 13, 8669– 8694, https://doi.org/10.5194/acp-13-8669-2013,
784   2013.

785 Schönhardt, A., Richter, A., Wittrock, F., Kirk, H., Oetjen, H., Roscoe, H. K., and Burrows, J. P.:
786   Observations of iodine monoxide columns from satellite, Atmos. Chem. Phys., 8, 637–653,
787   doi:10.5194/acp-8-637-2008, 2008.

788 Simó, R.: Production of atmospheric sulfur by oceanic plankton: biogeochemical, ecological and
789   evolutionary links: Trends. Ecol. Evol., 16, 287– 294, https://doi.org/10.1016/S0169-
790   5347(01)02152-8, 2001.

791 Stroeve, J. C., Jenouvrier, S., Campbell, G. G., Barbraud, C., and Delord, K.: Mapping and assessing
792   variability in the Antarctic marginal ice zone, pack ice and coastal polynyas in two sea ice
793   algorithms with implications on breeding success of snow petrels, The Cryosphere, 10, 1823–1843,
794   https://doi.org/10.5194/tc-10-1823-2016, 2016.

795 Ström, J., Engvall, A. C., Delbart, F., Krejci, R., and Treffeisen, R.: On small particles in the Arctic
796   summer boundary layer: observations at two different heights near Ny-Ålesund, Svalbard, Tellus B,
797   61, 473–482, 2009.

798 Suni, T., Kulmala, M., Hirsikko, A., Bergman, T., Laakso, L., Aalto, P. P., Leuning, R., Cleugh, H., Zegelin,
799   S., Hughes, D., van Gorsel, E., Kitchen, M., Vana, M., Hõrrak, U., Mirme, S., Mirme, A., Sevanto,
800   S., Twining, J., and Tadros, C.: Formation and characteristics of ions and charged aerosol particles
801   in a native Australian Eucalypt forest, Atmos. Chem. Phys., 8, 129–139,
802   https://doi.org/10.5194/acp-8-129-2008, 2008.

803 Svenningsson, B., Arneth, A., Hayward, S., Holst, T., Massling, A., Swietlicki, E., Hirsikko, A., Junninen,
804   H., Riipinen, I., Vana, M., Maso, M. D., Hussein, T., and Kulmala, M.: Aerosol particle formation
805   events and analysis of high growth rates observed above a subarctic wetland–forest mosaic, Tellus
806   B: Chem. Phys. Meteorol., 60, 353–364, https://doi.org/10.1111/j.1600-0889.2008.00351.x, 2008.

807 Teinilä, K., Frey, A., Hillamo, R., Tülp, H. C., and Weller, R.: A study of the sea-salt chemistry using size-
808   segregated aerosol measurements at coastal Antarctic station Neumayer, Atmos. Environ., 96, 11–
809   19, 2014.

810 Tremblay, S., Picard, J.-C., Bachelder, J. O., Lutsch, E., Strong, K., Fogal, P., Leaitch, W. R., Sharma, S.,
811   Kolonjari, F., Cox, C. J., Chang, R. Y.-W., and Hayes, P. L.: Characterization of aerosol growth
812   events over Ellesmere Island during the summers of 2015 and 2016, Atmos. Chem. Phys., 19, 5589–
813   5604, https://doi.org/10.5194/acp-19-5589-2019, 2019.

814 Vaughan, D. G., Marshall, G. J., Connolley, W. M., Parkinson, C., Mulvaney, R., Hodgson, D. A., King,
815   J. C., Pudsey, C. J., and Turner, J.: Recent rapid regional climate warming on the Antarctic Peninsula,
816   Climatic Change, 60, 243–274, https://doi.org/10.1023/a: 1026021217991, 2003.
817 Vehkamäki, H., Dal Maso, M., Hussein, T., Flanagan, R., Hyvärinen, A., Lauros, J., Merikanto, P.,
818   Mönkkönen, M., Pihlatie, K., Salminen, K., Sogacheva, L., Thum, T., Ruuskanen, T. M., Keronen,
819   P., Aalto, P. P., Hari, P., Lehtinen, K. E. J., Rannik, Ü., and Kulmala, M.: Atmospheric particle
820   formation events at Värriö measurement station in Finnish Lapland 1998–2002, Atmos. Chem.
821   Phys., 4, 2015–2023, https://doi.org/10.5194/acp-4-2015-2004, 2004.
822 Virkkula, A., Teinilä, K., Hillamo, R., Kerminen, V.-M., Saarikoski, S., Aurela, M., Viidanoja, J., Paatero,
823   J., Koponen, I. K., Kulmala, M.: Chemical composition of boundary layer aerosol over the Atlantic
824   Ocean and at an Antarctic site, Atmos. Chem. Phys., 6, 3407–3421, 2006.
825 Virkkula, A., Hirsikko, A., Vana, M., Aalto, P. P., Hillamo, R., and Kulmala, M.: Charged particle size
826   distributions and analysis of particle formation events at the Finnish Antarctic research station Aboa,
827   Boreal Environ. Res., 12, 397–408, 2007.
828 Weber, R. J., Marti, J. J., McMurry, P. H., Eisele, F. L., Tanner, D. J., and Jefferson, A.: Measurements
829   of new particle formation and ultrafine particle growth rates at a clean continental site, J. Geophys.
830   Res., 102, 4375–4385, 1997.
831 Weber, R. J., McMurry, P. H., Mauldin, L., Tanner, D. J., Eisele, F. L., Brechtel, F. J., Kreidenweis, S. M.,
832   Kok, G. L., Schillawski, R. D., and Baumgardner, D.: A study of new particle formation and growth
833   involving biogenic and trace gas species measured during ACE 1, J. Geophys. Res.-Atmos., 103,
834   16385–16396, https://doi.org/10.1029/97jd02465, 1998.
835 Weller, R., Minikin, A., Wagenbach, D., and Dreiling, V.: Characterization of the inter-annual, seasonal,
836   and diurnal variations of condensation particle concentrations at Neumayer, Antarctica, Atmos.
837   Chem. Phys., 11, 13243–13257, https://doi.org/10.5194/acp-11-13243-2011, 2011.
838 Weller, R., Schmidt, K., Teinilä, K., and Hillamo, R.: Natural new particle formation at the coastal
839   Antarctic site Neumayer, Atmos. Chem. Phys., 15, 11399–11410, https://doi.org/10.5194/acp-15-
840   11399-2015, 2015.
841 Weller, R., Legrand, M., and Preunkert, S.: Size distribution and ionic composition of marine summer
842   aerosol at the continental Antarctic site Kohnen, Atmos. Chem. Phys., 18, 2413–2430,
843   https://doi.org/10.5194/acp-18-2413-2018, 2018.
844 Williamson, C. J., Kupc, A., Axisa, A., Kelsey R., Bilsback, K. R, Bui, T. P., Campuzano-Jost, P., Dollner,
845   M., Froyd, K. D., Hodshire, A. L., Jimenez, J. L., Kodros, J. K., Luo, G., Murphy, D. M., Nault, B.
846   A., Ray, E. A., Weinzierl, B., Wilson, J. C., Yu, F., Yu, P., Pierce, J. R., and Brock, C. A.: A large
847   source of cloud condensation nuclei from new particle formation in the tropics, Nature, 574, 399–
848   403, https://doi.org/10.1038/s41586-019-1638-9, 2019.
849 Yli-Juuti, T., Riipinen, I., Aalto, P. P., Nieminen, T., Maenhaut, W., Janssens, I. A., Claeys, M., Salma, I.,
850   Ocskay, R., Hoffer, A., Imre, K., and Kulmala, M.: Characteristics of new particle formation events
851   and cluster ions at K-puszta, Hungary, Boreal Environ. Res., 14, 683–698, 2009.
852 Yu, F. and Luo, G.: Oceanic dimethyl sulfide emission and new particle formation around the coast of
853   Antarctica: a modeling study of seasonal variations and comparison with measurements,
854   Atmosphere, 1, 34–50, 2010
855 Zheng, G., Wang, Y., Wood, R., Jensen, M. P., Kuang, C., McCoy, I. L., Matthews, A., Mei, F., Tomlinson,
856   J. M., Shilling, J. E., Zawadowicz, M. A., Crosbie, E., Moore, R., Ziemba, L., Andreae, M. O., and
857   Wang, J.: New particle formation in the remote marine boundary layer. Nat Commun. 12(1), 527.
858   doi: 10.1038/s41467-020-20773-1, 2021.
859 Zhu, R. B., Sun, J. J., Liu, Y. S., Gong, Z. J., and Sun, L. G.: Potentialammonia emissions from penguin
860   guano, ornithogenic soils and seal colony soils in coastal Antarctica: effects of freezingthawing
861   cycles and selected environmental variables, Antarct. Sci., 23, 78–92,
862   doi:10.1017/s0954102010000623, 2011.

Table 1. Total particle number concentration > 10 nm (CN_{10}), particle number concentrations of the nucleation mode (N_{NUC}), Aitken mode (N_{AIT}), accumulation mode (N_{ACC}), CCN number concentration at supersaturation of 0.4% ($CCN_{0.4\%}$), and metrological parameters solar radiation, temperature, RH, pressure, wind speed, and wind direction for 2018.

	CN_{10} (cm^{-3})	N_{NUC}[a] (cm^{-3})	N_{AIT}[a] (cm^{-3})	N_{ACC}[a] (cm^{-3})	$CCN_{0.4\%}$ (cm^{-3})	Solar radiation (W m^{-2})	Temp. (°C)	RH (%)	Pressure (hPa)	Wind Speed (m sec^{-1})	Wind direction (°)
January	506.2	101.1	188.7	83.8	235.2	129.2	1.1	88.6	986.0	5.78	315.8
February	594.3	111.3	200.0	69.9	229.8	103.5	1.8	90.8	987.2	7.72	319.9
March	357.3	86.0	112.4	42.1	138.7	58.0	1.1	88.4	981.8	8.21	342.3
April	184.1	49.9	39.1	17.5	58.6	26.2	-0.7	87.1	988.2	7.88	350.0
May	106.7	25.1	23.8	14.2	51.1	7.3	-2.3	81.8	990.1	7.34	277.7
June	75.9	12.2	12.5	9.2	35.4	3.4	-4.1	88.4	995.9	7.21	339.8
July	84.3	28.2	16.8	11.6	39.1	5.5	-2.9	86.5	992.2	9.08	300.8
August	109.8	39.3	19.6	14.8	52.1	21.8	-3.3	85.9	986.2	8.57	327.8
September	266.4	123.8	51.3	20.9	79.3	65.6	-3.6	86.5	992.6	9.52	313.2
October	287.0	88.9	62.0	26.9	105.3	122.1	-2.1	84.6	994.4	6.50	290.8
November	498.2	79.3	136.8	46.1	150.3	143.3	-0.6	89.3	980.0	7.59	307.9
December	511.9	193.5	227.6	67.7	189.1	136.5	0.4	87.2	980.4	6.72	302.7

[a]N_{NUC}, N_{AIT}, and N_{ACC} represent the particle number concentrations in the nucleation mode (3–25 nm), Aitken mode (25–100 nm), and accumulation mode (100–300 nm).
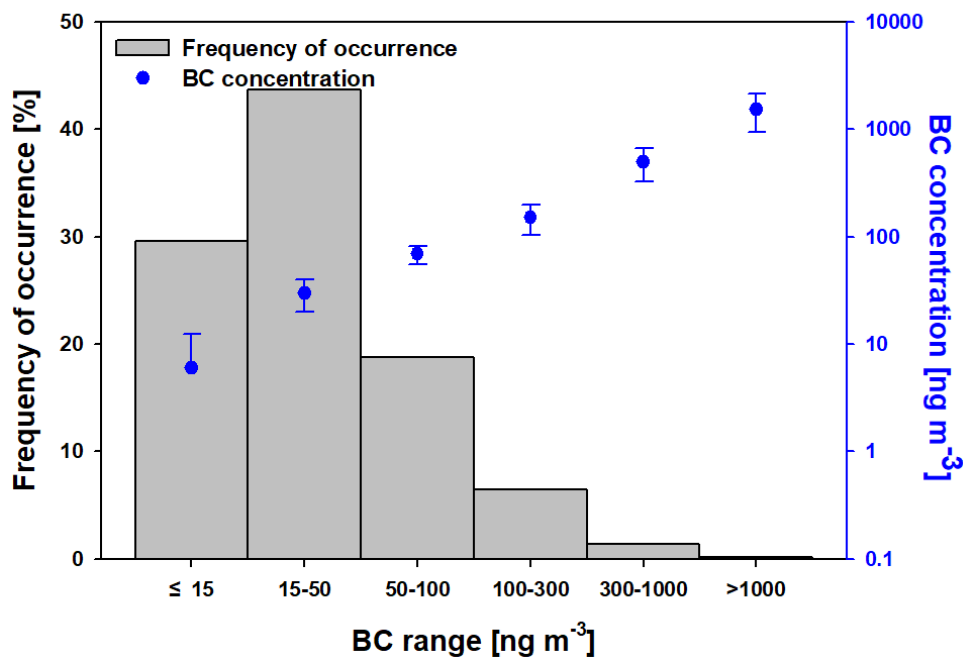
Figure 1. Frequency of occurrence of BC mass concentration for six types of Antarctic Peninsula air-pollution levels classified from four-year BC data.
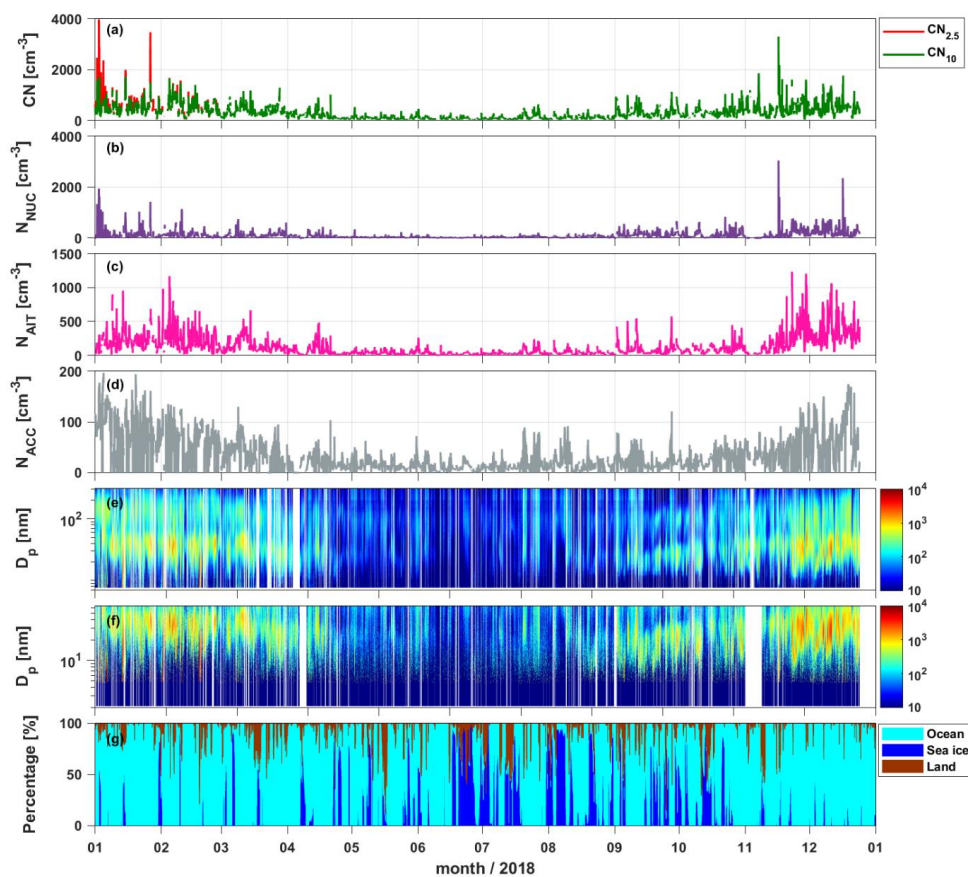
Figure 2. Time series of 1 h averages for (a) total aerosol (CN$_{2.5}$ and CN$_{10}$), (b) nucleation mode

(N$_{NUC}$; 3–25 nm), (c) Aitken mode (N$_{AIT}$; 25–100 nm), and (d) accumulation mode (N$_{ACC}$; 100–

300 nm); contour plots of the size distributions measured using (e) standard and (f) nano-SMPS;

and (g) residence time of air masses passing over ocean, sea ice, and land. CN$_{2.5}$ and CN$_{10}$

represent total number concentration of particles > 2.5 (measured using TSI 3776 CPC) and 10

nm (measured using TSI 3772 CPC), respectively.
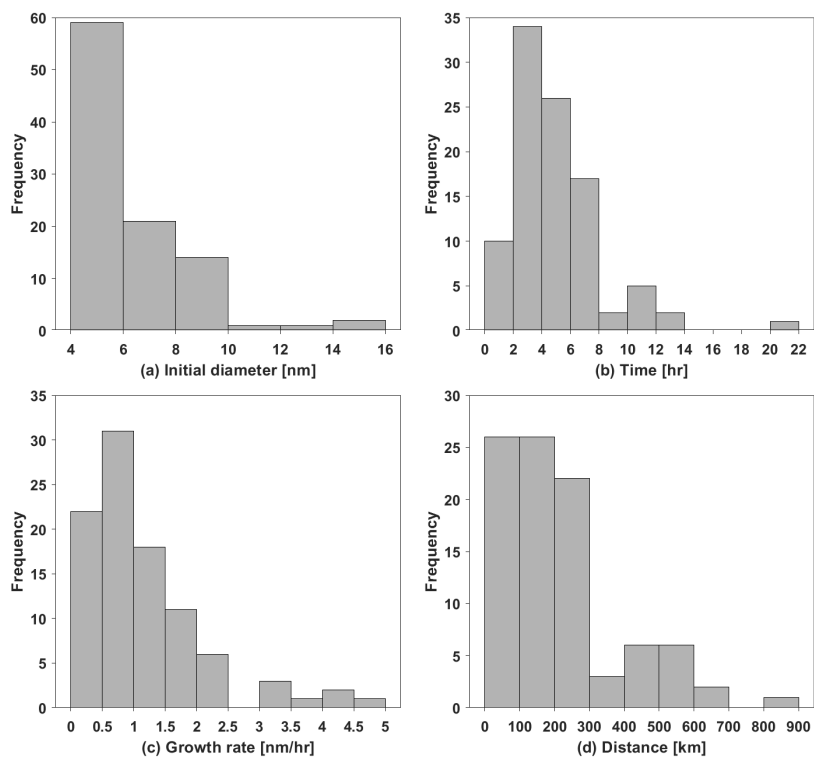
Figure 3. Frequency of (a) initial diameter of particles, (b) duration time, (c) growth rate, and (d) extension for the NPF event. Two NPF cases were excluded when the wind speed was higher than 10 ms⁻¹.
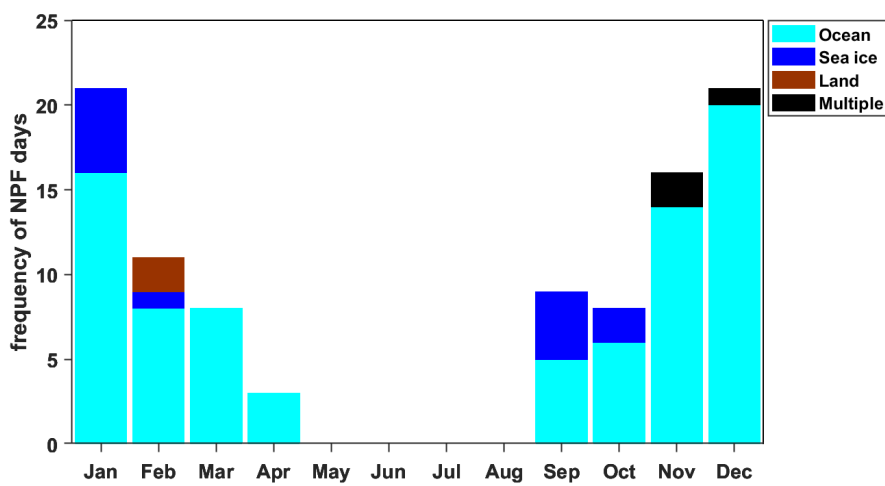
Figure 4. Seasonal variations in the number of NPF days by air mass origin.
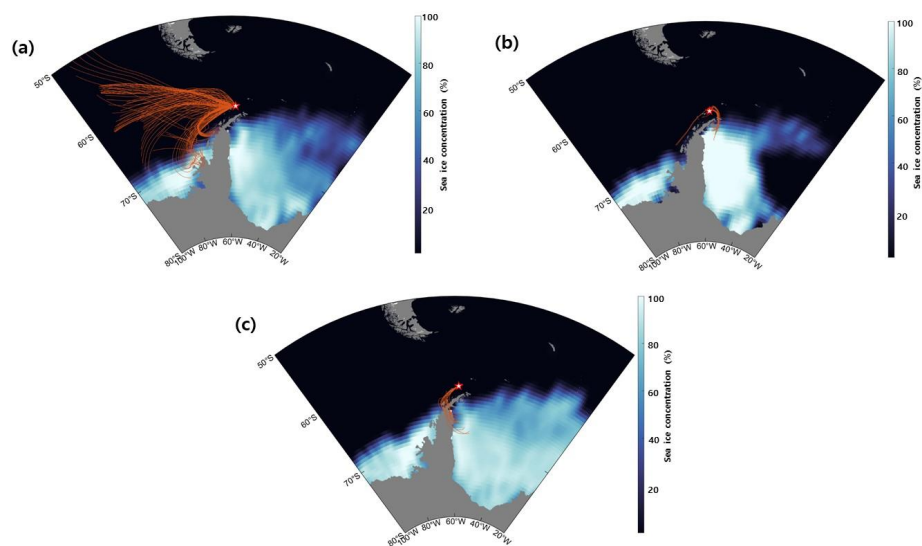
Figure 5. Air mass back trajectories for arrival at 50 m for the four case study NPF events: (a) marine, (b) sea ice, and (c) multiple.
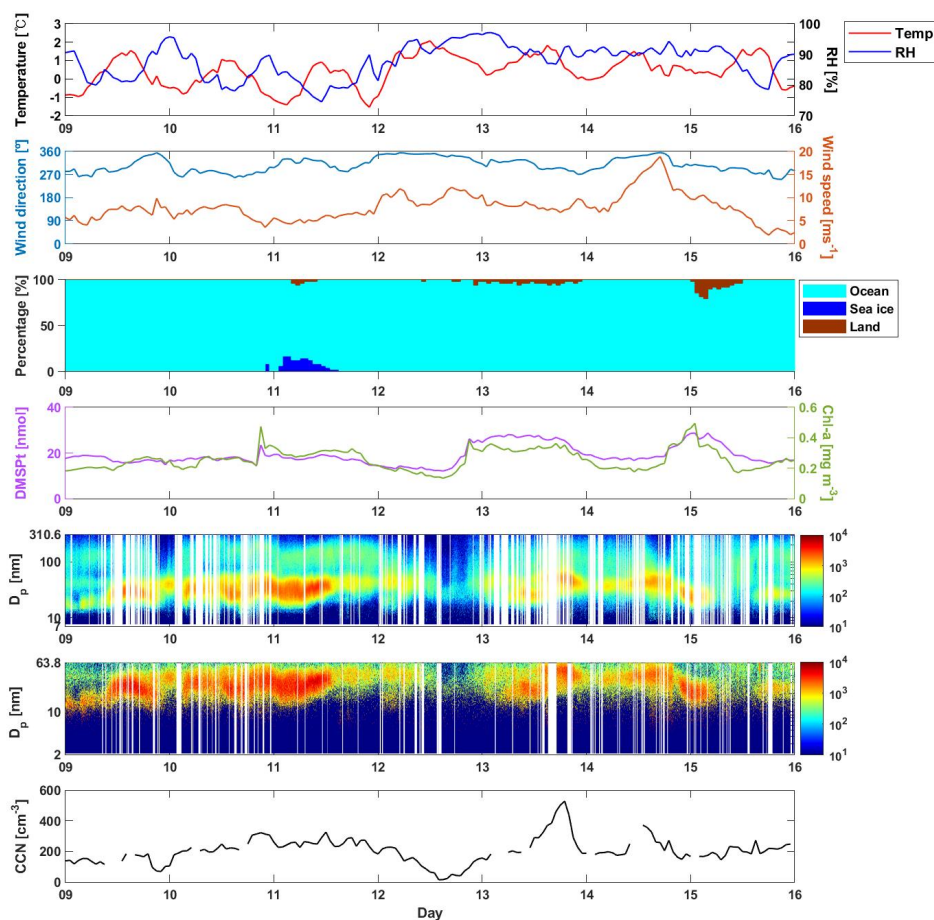
Figure 6. Marine NPF event observed from December 9–15, 2018. From top to bottom, the parameters are as follows: meteorological variables, the residence time of air masses that passed over the ocean, sea ice and land areas, number size distribution with the standard-SMPS and nano-SMPS, and CCN number concentration.
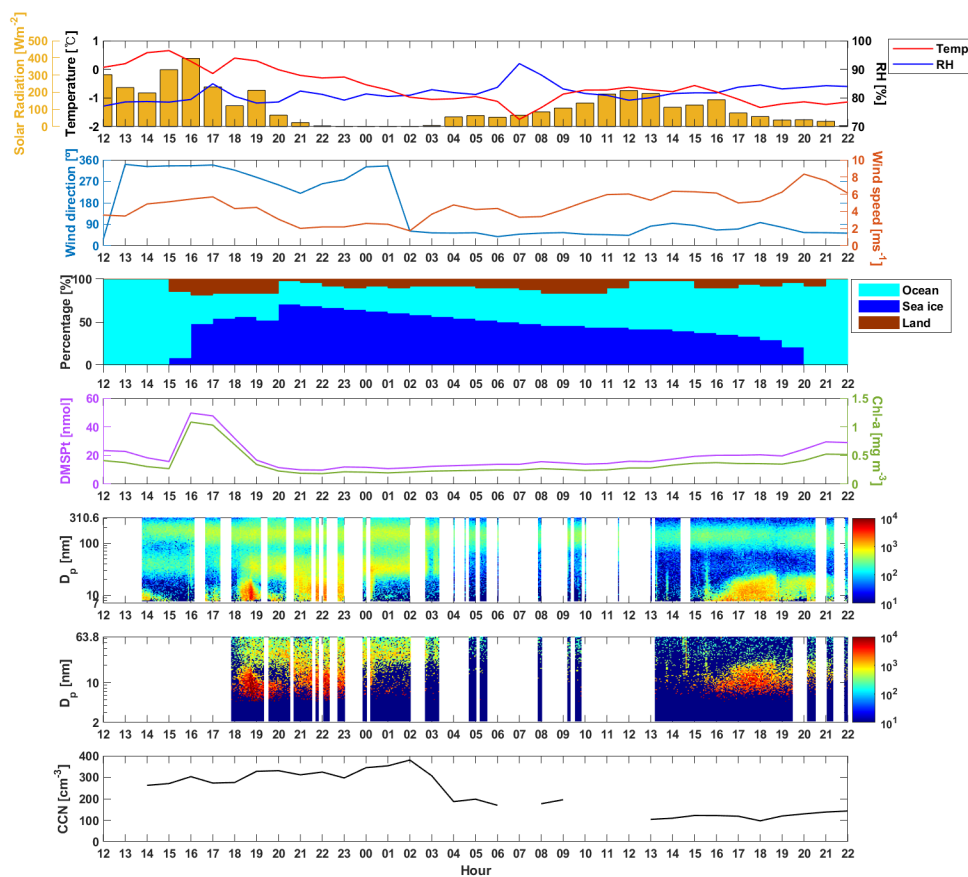
Figure 7. Sea ice NPF event observed from January 2–3, 2018. From top to bottom, the parameters are as follows: meteorological variables, the residence time of air masses that passed over the ocean, sea ice and land areas, number size distribution with the standard-SMPS and nano-SMPS, and CCN number concentration.
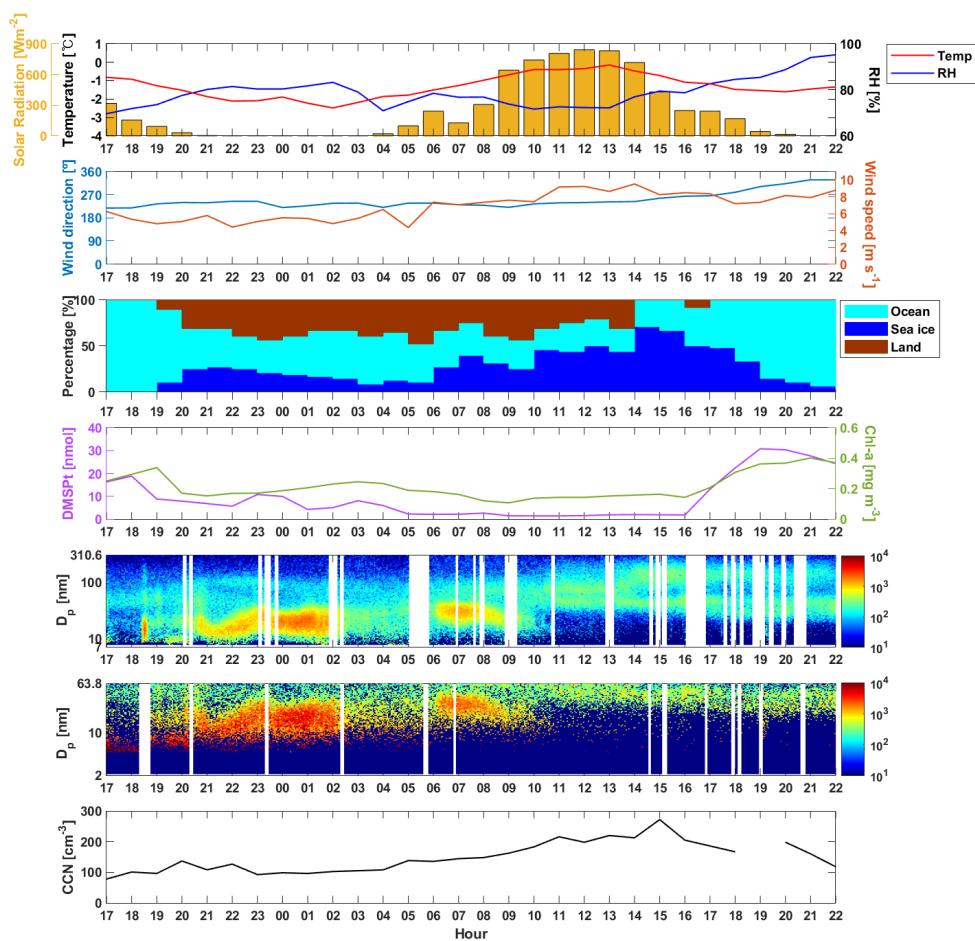
Figure 8. Multiple NPF event observed from November 16–17, 2018. From top to bottom, the parameters are as follows: meteorological variables, the residence time of air masses that passed over the ocean, sea ice and land areas, number size distribution with the standard-SMPS and nano-SMPS, and CCN number concentration.
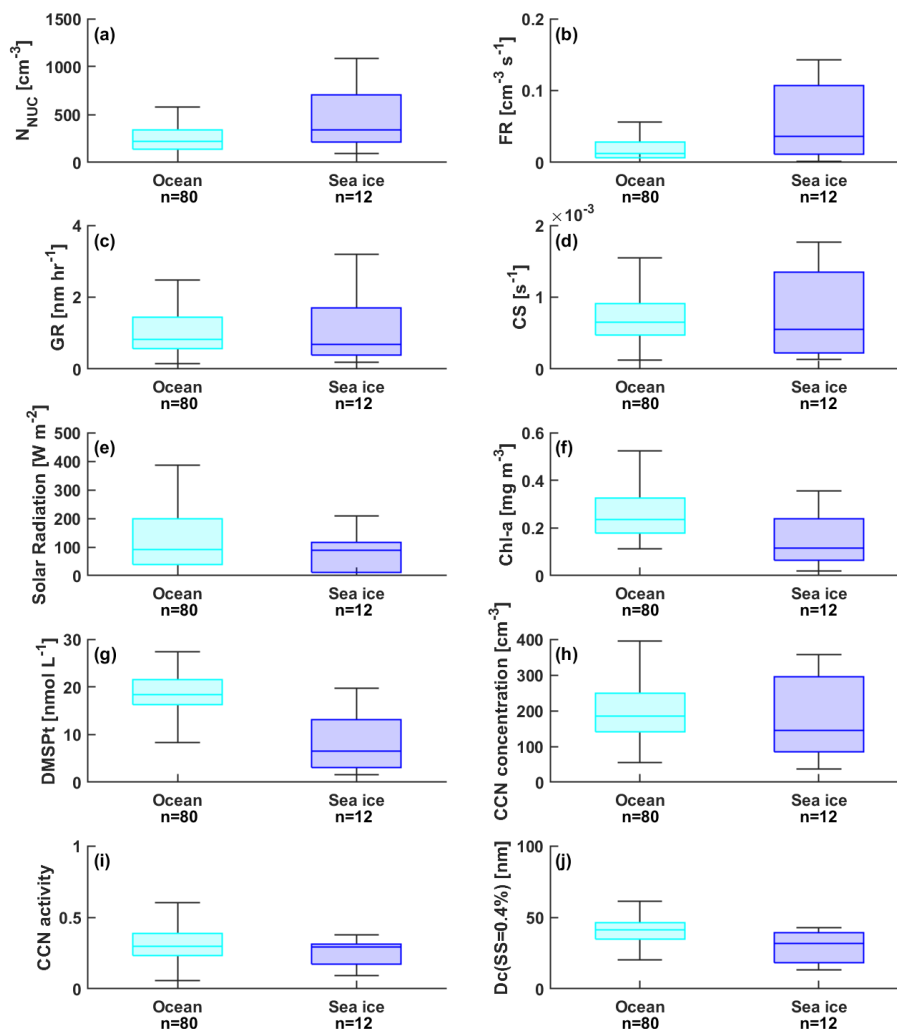
Figure 9. Box plots for (a) number concentration of nucleation-mode particles (N_{NUC}), (b) formation rate for, (c) growth rate (GR), (d) condensation sink (CS), (e) solar radiation, (f) chlorophyll exposure, (g) DMSP exposure, (h) CCN number concentration, (i) CCN activity, and (j) critical diameter (D_c) for ocean, sea ice, and multiple air masses. Upper/lower box limits and solid lines indicate the 75th/25th percentiles and median, respectively.